

The Spiral Structure of Our Galaxy Determined from H II Regions

Y. M. Georgelin and Y. P. Georgelin

Observatoire de Marseille, Observatoire de Haute Provence

Received July 3, 1975, revised January 22, 1976

Summary. The overall, large-scale distribution of ionized hydrogen regions in our Galaxy defines a spiral structure comparable to the large-scale spiral patterns observed in external galaxies. In order to outline the spiral arms of our Galaxy we have combined our optical observations (distances of exciting stars and H α radial velocities) with the radio observations of H II regions [H 109 α radial velocities (Mezger, 1970)], using a method proposed by Bok (1971). Our new observations of the radial velocities of 268 H α regions and new distance determinations for 360 exciting stars, have allowed us to define a detailed rotation model exhibiting, in certain sectors, deviations from circular motion, thus permitting us to correctly fit together the stellar and kinematic distances; this rotation model has been supplemented, in the interior part of the Galaxy (galactocentric distance between 4 and 5 kpc, longitudes 330° to 340°) by using H 109 α velocity maxima. The optical detection of very distant H II regions—out to 9 kpc of the Sun—has permitted a good overlap be-

tween the optical data and the H 109 α radio data (obtained over the whole of our Galaxy with nevertheless a distance selection effect as shown in Fig. 11). In addition, we have analyzed the radial velocities and made precise identifications (using H α photographs and radio continuum maps) so as to group together all the H 109 α sources of a single complex. These identifications, along with the use of radio absorption components (molecules, 21-cm), have allowed us to resolve the distance ambiguity for all these H II complexes (with a high certainty for 66%). Eighty per cent of the high-excitation-parameter H II regions thus defined fall along two symmetrical pairs of arms (i.e. four altogether) of 12° inclination. The longitudes at which one sees these arms tangentially correspond exactly to the flux maxima in the radio continuum and in the total 21-cm profile integral.

Key words: H II regions — spiral structure

I. Introduction

In the past it was impossible to reconcile the models of the spiral structure of our Galaxy established from optical results with those based on radio observations. There were a number of reasons for this.

The older optical observations were limited to the solar neighborhood, and the resulting interpretations of structure attributed undue importance to this part of the Galaxy.

Observations at radio wavelengths have the advantage of not being limited by interstellar absorption, thus permitting exploration of the entire Galaxy. The 21-cm line observations, in particular, give the column density of neutral hydrogen integrated along a line of sight as a function of the radial velocity. However, these neutral hydrogen observations have a number of shortcomings. Two of these are common to all kinematic methods of spiral structure determination. They are, first, the necessity of using a rotation model to transform the radial velocities to distances. The determination of such a model is plagued by non-circular motions (Shane and Bieger-Smith, 1966; Kerr, 1970; Burton, 1973):

small fluctuations (~ 1 kpc) and larger scale variations as a function of galactocentric longitude (i.e., the difference between the northern and southern hemispheres as has been shown by Kerr, 1970). Second, for the interior parts of the Galaxy the rotation model gives two possible distances for a given observed radial velocity, and it is sometimes difficult to choose between the “near” and the “far” distance. In addition, the 21-cm observations have the particular shortcoming of resulting from an integration along the line of sight. Burton (1973) has shown that “In fact it is not clear to what extent a particular peak in a line profile owes its characteristics to streaming motions, to a density concentration or to a variation in temperature”. This means that the spiral arms cannot be determined with any accuracy directly from 21-cm line data. This shortcoming does not exist in the case of observations of discrete H II regions.

In recent years much progress has been made in the spiral structure problem: (i) important new optical data has been obtained (OB stars and H II regions)

especially in the southern hemisphere, (ii) radio-recombination lines have been discovered and extensively observed (Mezger, 1970; Reifenstein *et al.*, 1970; Wilson *et al.*, 1970 etc.) as have the radio molecular lines (Manchester *et al.*, 1970; Goss *et al.*, 1969; Robinson *et al.*, 1971; Caswell and Robinson, 1974; Wilson, 1972 etc.), (iii) a model-fitting approach has been applied to the interpretation of the 21-cm profiles (Burton and Shane, 1970), and new analyses of H I data in terms of the gravitational theory of density-waves has been done (Burton, 1973).

The purpose of this article is to try to establish *from the study of a homogeneous population—H II regions and their exciting stars—a coherent schema of the spiral structure of our Galaxy* which is compatible with the optical and the radio results. This method, recommended by Bok (1971), has been successfully used in the Carina arm by Bok *et al.* (1970). We shall try here to generalize it to the entire Galaxy as it has been briefly shown by Georgelin (1975a). To do this we use our new determinations of distances of exciting stars and of H α radial velocities (Georgelin, 1975), as well as all available H 109 α radial velocities and particularly those of Reifenstein *et al.* (1970) and of Wilson *et al.* (1970).

Our new observational results have also permitted us to greatly extend the optical exploration zone, particularly in Cygnus and in Carina (up to 8 and 9 kpc). This considerably increases the region of overlap of the optical with the radio results, and therefore facilitates the harmonisation of the two.

For this synthesis, based primarily on H II regions and exciting stars, we have also used the results for other optical constituents (supergiants, young clusters) and radio constituents (H I, molecules) of Population I. To do this we had to examine all the optical and radio data in detail, nebula by nebula. This work was simplified in the Carina region and in the Crux-Centaurus-Norma region by the extensive contributions in the catalogues of Hine (1971) and Smith (1972).

II. Method of Analysis

1. Observational Data: Accuracy and Homogeneity

To have any hope at all of defining the spiral structure of our Galaxy, one must use a distance scale (spectrophotometric and kinematic) based on data which are as homogeneous and accurate as possible. The radial velocities of H α regions have been measured by the Fabry-Perot interferometric method described by Courtès (1960); thus, at a mean reciprocal dispersion of 20 Å mm⁻¹, we have measured the H α radial velocities of about 8000 elements of a few square seconds-of-arc in 268 H II regions distributed quasi-uniformly over the entire galactic plane. The spectrophotometric distances of the 360 exciting stars of these H II regions have been obtained from spectral classifications and *UBV* photo-

metry effectuated by about fifty different authors, principally Crampton (1971), Crampton and Fisher (1974), and Georgelin *et al.* (1973). The absolute magnitude-spectral type calibration which we use (Crampton and Georgelin, 1975) takes into account important advances made by Conti and Alschuler (1971), Walborn (1972), and Balona and Crampton (1974).

All of the observational results, the critical analysis of the spectral classifications and absolute magnitudes, as well as a detailed study of the exciting OB clusters have been assembled by Georgelin (1975).

In this work we have extensively used the H 109 α radial velocities observed by Reifenstein *et al.* (1970), Wilson *et al.* (1970), Caswell (1972), Dickel and Milne (1972).

2. Grouping of the Various Measurements

Because of the intrinsic scatter of radial velocity within each H II region—i.e., $\sigma = 4.2$ km s⁻¹ (Table 1)—it is not correct to derive a kinematic distance from each measurement, at the risk of finding a spiral structure more confused than the reality. Therefore the observations are judiciously grouped and one distance is derived for each H II region or each complex H II region from mean radial velocity. One must exercise great care to define real physical groupings; we have done this with the aid of H α photographs and radio continuum maps. Thus, for example, the 36 H II regions detected in radio at $\ell = 332^\circ$ and $\ell = 337^\circ$ have been grouped into nine H II complexes of various sizes, allowing—finally—the structural interpretation of this crucial zone of the Galaxy.

3. Rotation Model

Relatively recent studies (as Courtès *et al.*, 1967) of the detailed and accurate kinematics of the large nearby galaxies has shown that they present great irregularities, on both a large scale and on a small scale, of the rotational velocity Θ as a function of R (distance from the galactic center) and of L (galactocentric longitude); the situation is the same in our Galaxy. Consequently we have tried to define separate rather detailed rotation models for two zones of galactocentric longitude, in order to best tie in the kinematic distances with the spectrophotometric distances. In the optical zone we have used the distances of the exciting stars and the radial velocities of the H α regions, and in the interior parts of the Galaxy the maximum velocities of the H 109 α regions.

4. Ambiguity of the Distances

For the internal parts of the Galaxy the choice between the two distances corresponding to the same observed radial velocity was made with the aid of the following

complementary information, listed in order of decreasing certitude:

- (1) The distance of the exciting star. If known, all ambiguity is removed.
- (2) The fact that an H II region is observed optically. This is an argument in favor of the "near" solution.
- (3) Absorption components of radio lines, at greater absolute velocities than that of the H II region are evidence in favor of the "far" solution.
- (4) The fact that an H 109 α region is not observed optically is an argument in favor of the "far" solution.
- (5) The latitude thickness of the arm. If the latitude range is large, the "far" distance is unacceptable.
- (6) Absorption components of radio lines at smaller absolute velocities than that of the H II region are evidence slightly in favor of the "near" distance.
- (7) The velocity continuity along the arms or the continuity of the arms. As observation of external galaxies demonstrates, arms have a spiral shape with pitch angles varying from 0° to 30°; the sense of this inclination is known for our Galaxy. In the absence of other indications of the distance (near or far), we choose the solution permitting the alignment of the H II regions along spirals of plausible inclination. There is ambiguity of distance for 67 H II regions among the 100 important H II regions. This ambiguity is resolved with a high certainty for 44 H II regions (criteria 1 to 4) and with a lower certainty for 23 H II regions (criteria 5 to 7). Details are given in Table 10.

5. Weighting of the H II Regions

The H II regions which trace the spiral arms in external galaxies are "important" (brilliant and extended). In order to trace the spiral arms in our Galaxy it is therefore best to place ourselves in the same conditions as the observer of external galaxies, as has been suggested by Bok (1969). The most representative criterion of the "importance" of the H II regions is the excitation parameter U ; U is proportional to $(SD^2)^{1/3}$, where S is the radio flux emitted by the H II region and D is its distance. In this study we have therefore selected and weighted the H II regions in such a way as to favor the largest excitation parameters, so as to simulate the observational conditions for external galaxies, and to reduce the selection effect due to distance from the Sun.

6. External Galaxies

In this paper we try to establish, from the study of H II regions, a coherent scheme of the spiral structure of our Galaxy. We need guidance in this analysis from the results of studies of the neighboring galaxies. For the optical astronomers it is easy to obtain the distribution of H II regions in spiral galaxies; these studies can be made with great precision in M 31 (Arp, 1964) and

Table 1. Dispersions of radial velocities

Scale	Standard deviation (km s ⁻¹)
Within an individual H II region	4.2
Between H II regions of an element of spiral arm (500 pc)	4.5
Between H II regions of an entire spiral arm (5000 pc)	7.4
Between H II regions within a radius of 5 kpc around the sun	6.7

in M 33 (Boulesteix *et al.*, 1974). From the observations of H II regions in external galaxies we can conclude:

— that the arms are observed approximatively between $R=3$ and $R=12$ kpc;

— that the pitch angle (Danver, 1942) is:

for Sb galaxies $\mu=75^\circ 2$ with $\sigma_{r.m.s.}=5^\circ 9$ and for Sc galaxies $\mu=72^\circ 5$ with $\sigma_{r.m.s.}=6^\circ 4$ and

— that there is a very precise symmetry in the spiral arm pattern, especially in the inner regions, and particularly for M 33, M 51 and M 31, but that these galaxies are not symmetrical in their kinematic properties but instead exhibit very significant non-circular motions.

Moreover, H I observations in external galaxies show that the H I spiral arms are strong in the outer parts of the galaxies where H II regions are inconspicuous, and vice versa in the inner parts.

III. Rotation Model—Kinematic Distances

The determination of a rotation model from the radial velocities of H II regions is possible because of the sufficiently weak dispersion of these velocities. Table 1 shows the standard deviations found on different scales.

In various papers (Georgelin and Georgelin, 1970b; Georgelin, 1975; Crampton and Georgelin, 1975) we have studied the kinematics of optical H II regions (U_0 , V_0 , A , α , R_0 , etc.) with extensive comparison with the results obtained by several authors for stellar Population I objects. From our radial velocities of H II regions we have also made a tentative (Georgelin, 1975) approach to involve streaming motions along the spiral arms in terms of density-wave theory for the gas (Roberts, 1969). But in this paper we limit the kinematic study to the critical parameters used for kinematic distance determination.

1. Mean Rotation Curve

For 151 optical H II regions we have obtained both the radial velocity of the H II region and the spectrophotometric distance of the exciting star (s). From these data, with $R_0=10$ kpc, we have calculated by means of a least-

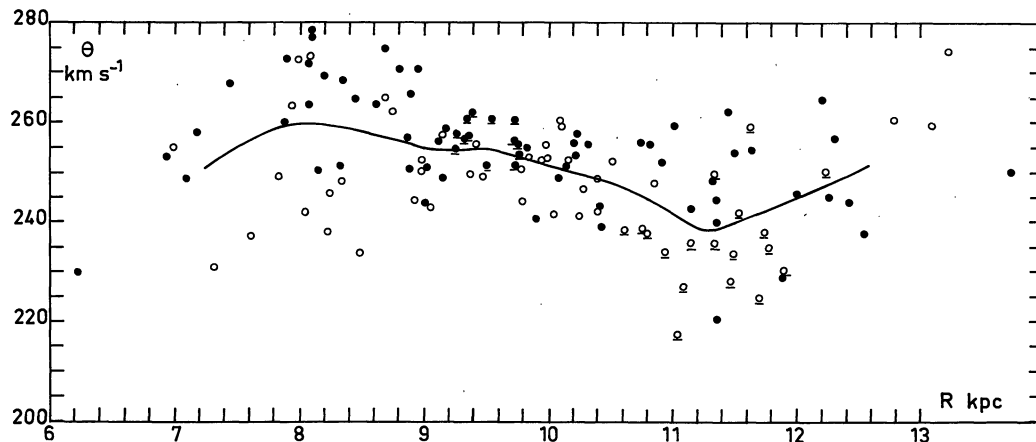


Fig. 1. Rotation curve of our Galaxy calculated from distances of exciting stars and radial velocities of H α regions. The abscissa represents the distance from the galactic center and the ordinate the rotation velocity. Underlined open circles corresponds to Perseus feature and underlined filled circles correspond to Carina feature. \bullet : $\ell > 180^\circ$; \circ : $\ell < 180^\circ$

squares method: $U_0 = -7.2 \text{ km s}^{-1}$ and $V_0 = +14.7 \text{ km s}^{-1}$. In this paper the rotation model and all the distances have been computed with these values (V_{HII}), even if we have given the V_{LSR} radial velocities for easier comparison. Figure 1 gives, for each H α region, the rotation velocity Θ around the galactic center, calculated in the classical way by

$$\Theta = (R/R_0) (\Theta_0 + V_{\text{HII}}/\sin \ell)$$

and

$$R^2 = R_0^2 + r^2 - 2r R_0 \cos \ell,$$

where R and $R_0 = 10 \text{ kpc}$ are the galactocentric distances of the H II region and of the Sun, respectively; Θ and $\Theta_0 = 250 \text{ km s}^{-1}$ are the rotational velocities around the galactic center; r is the distance to the exciting star; and V_{HII} is the radial velocity of the H II region corrected for the solar motion. The northern H II regions ($0^\circ < \ell < 180^\circ$) are represented by open circles, and the southern H II regions ($180^\circ < \ell < 360^\circ$) by filled circles. The mean curve was found by taking a running mean, weighted by $\sin \ell$, over groups of ten points. The mean rotation curve differs from the Schmidt model (Schmidt, 1965) by:

- (1) a maximum around 8 kpc;
- (2) a minimum around 11.3 kpc (Perseus arm);
- (3) an increase for $R > 12 \text{ kpc}$.

These last two points have already been noted by Humphreys (1970), Balona and Feast (1974), and Georgelin (1975) respectively for supergiants, OB stars, and H II regions.

The last point has also been noted by Burton and Bania (1974). They show the response of the correlation coefficient ρ (correlation between the observed deviations from circular motion and the model non-circular motions calculated at the locations of the observed objects) to variations in the parameter k specifying the model basic rotation curve. This correlation analysis (Burton and Bania, 1974) is made for associations, supergiants and H II regions, and the results are very

conclusive for H II regions where the correlation is certainly significant despite the limited number of regions used. The maximum correlation is obtained for a basic rotation curve characterized by $k = +3$ instead of $k = 0$ (Schmidt model). From H II regions we obtain (Fig. 2), for $12 < R < 13 \text{ kpc}$, $\Theta = 250 \text{ km s}^{-1}$, corresponding to $k = +3$ in agreement with Burton and Bania (1974).

2. North-south Discontinuity from Optical Results

A detailed, point-by-point analysis of Fig. 1 shows that the southern hemisphere points ($180^\circ < \ell < 360^\circ$) tend to have a greater rotational velocity. In order to confirm this, we have separated the northern and southern points and smoothed in the same way as for the mean curve. Figure 2, on which we have indicated the root-mean-square dispersions of these two rotation curves, confirms their clear separation, particularly for 8.5 kpc and for 11.2 kpc. It is important to remember that this effect (southern rotation faster than northern rotation) is in the same sense as that observed in H I by Kerr (1970) between 8.2 and 10 kpc. We also note that from 7 kpc to 10 kpc the northern curve is very close to the Schmidt model, while the southern curve is located significantly above, the difference reaching 14 km s^{-1} at 8.3 kpc; beyond 12 kpc the curves are less well defined, but the northern and southern curves seem to be identical while remaining above that of the Schmidt model.

In an extensive work on supergiants, Humphreys (1970) has shown that their kinematics in the longitude sector $30^\circ < \ell < 210^\circ$, are different from those in the sector $210^\circ < \ell < 30^\circ$. A re-analysis of her data, in the same manner as for the H II regions, shows that the effect for the supergiants is indeed in the same sense as that for H II regions—i.e., the rotation curve for the southern hemisphere ($180^\circ < \ell < 360^\circ$) is located above that for the northern hemisphere ($0^\circ < \ell < 180^\circ$).

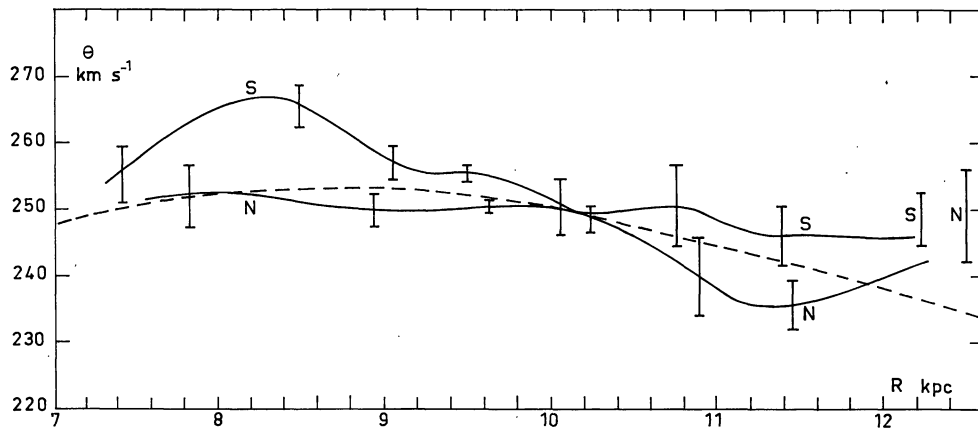


Fig. 2. Rotation curves of our Galaxy calculated from distances of exciting stars and radial velocities of H α regions for longitudes $0^\circ < \ell < 180^\circ$ (north) and $180^\circ < \ell < 360^\circ$ (south). The dotted line represents the Schmidt model

3. Deviations from Circular Motion. Carina Section and Perseus Section

Two undisputed features in the Population I structure of our Galaxy are the so-called “Carina section” and “Perseus section”. The “Carina section” (with $2.5 < r < 8$ kpc, $1282^\circ < \ell < 286^\circ$, $9 < R < 10.5$ kpc, external longitude $\ell = 282^\circ$) was extensively studied by Bok *et al.* (1970), and the “Perseus section” (with $100^\circ < \ell < 150^\circ$, $2 < r < 3$ kpc, $11 < R < 12$ kpc) was discovered by Morgan *et al.* (1952) from OB stars and by Oort *et al.* (1958) from H I observations.

The analysis of the rotation curve (Fig. 2) shows, first, that the points of the “Carina section” between $9 < R < 10$ kpc are located even higher than the southern rotation curve; and second, that the points of the Perseus arm (10.8 kpc $< R < 11.8$ kpc) are located lower than the northern rotation curve, which confirms the deviation from circular rotation already well known for these two regions. From our values we have determined, for the Carina arm (9.1 kpc $< R < 9.5$ kpc), a slope $A = 19$, which corresponds to a deviation from circular rotation of ($\Delta V = -2A(R - R_0) \sin \ell \approx 6$ km s $^{-1}$), an effect already observed for H II regions (Bigay *et al.*, 1972) and for hot stars (Humphreys, 1972; Burton and Bania, 1974, Fig. 2).

4. Rotation Curve of Ionized Gas from Radio Results for $3.9 < R < 5$ kpc

Between $\ell = 330^\circ$ and $\ell = 339^\circ$ the H 109 α results of Wilson *et al.* (1970, Fig. 1, p. 380) show two alignments of numerous H II regions at $\ell = 332^\circ$ and $\ell = 337^\circ$. These two typical alignments show a “hole” of 4 kpc around the tangential point which could mean either that there are no H II regions in this zone—in which case we would have a rather curious 4 kpc interarm gap—or that the observed velocities are not as great as the maximum velocity predicted by the Schmidt model.

Table 2. Maximum radial velocities observed near 335°

Component	V_{LSR}	Reference
H 109 α	-93, -91, -89, -89, -88	Wilson <i>et al.</i> (1970)
OH absorption	-89, -88	Goss <i>et al.</i> (1970)
CH $_2$ O	-90, -85	Whiteoak and Gardner (1970)
Interstellar Ca absorption	-94, -82, -82, -82	Chu-Kit (1973)
	-82, -81	

Therefore, we have searched in the sector $330^\circ < \ell < 340^\circ$ for maximum velocities measured for each separate constituent. The results are given in Table 2.

We have deduced from these results a mean observed maximum velocity of -90 km s $^{-1}$ at $\ell = 332^\circ$, and -93 km s $^{-1}$ at $\ell = 337^\circ$. No significant error is introduced by considering this observed maximum velocity as the velocity at the tangential point, because two weak effects acting in opposing directions tend to compensate each other:

- (1) Because of the statistical scatter of the radial velocities, one risks overestimating the velocity of the tangential point by a few km s $^{-1}$ when one selects the maximum velocity observed.
- (2) There is not necessarily an H II region at the tangential point; thus the maximum measured velocity may correspond to a point located in front of or behind the tangential point, whose velocity, therefore, is underestimated.

The two maximum velocities obtained for the longitudes 332° and 337° allow modification of the rotation curve of our Galaxy for the southern hemisphere. With $V_{\text{LSR,max}} = -90$ km s $^{-1}$ at $\ell = 332^\circ$ and $V_{\text{LSR,max}} = -93$ km s $^{-1}$ at $\ell = 337^\circ$ one obtains, for the rotation velocities, $\Theta = 210$ km s $^{-1}$ and 193 km s $^{-1}$, respectively. These values are respectively 19 km s $^{-1}$ and 13 km s $^{-1}$ less than the rotation velocities predicted by the Schmidt model.

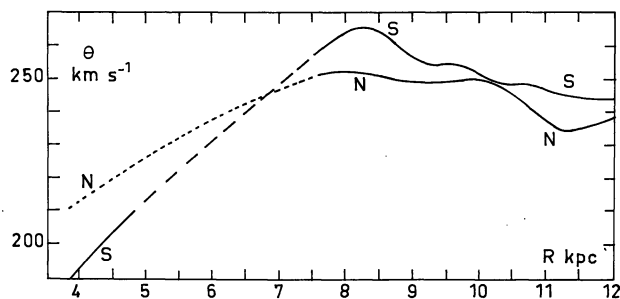


Fig. 3. Rotation curves of our Galaxy calculated from distances of exciting stars and radial velocities of $H\alpha$ regions for $7 < R < 12$ kpc and from $H 109\alpha$ velocity maxima for $3.9 < R < 5$ kpc in the southern hemisphere. Schmidt model for $R < 7$ kpc in the northern hemisphere. -----: Schmidt model; —: $H II$ regions

This is to be compared to the somewhat weaker asymmetry, in the same sense, of about 10 km s^{-1} observed at 21-cm by Kerr (1970) between the northern and southern hemispheres. The observed rotational dissymmetry ($\Delta\theta = 20 \text{ km s}^{-1}$) at $R = 4.5$ kpc, for which $\theta = 200 \text{ km s}^{-1}$, for points 65° apart with respect to the galactic center, is not particularly important if one compares this to the results obtained in external galaxies. For example, in M 33, for points diametrically opposed, $\Delta\theta = 40 \text{ km s}^{-1}$ at $R = 4$ kpc, for which $\theta = 70 \text{ km s}^{-1}$; and in the galaxy NGC 6946 (Sc multi-arm) it is even greater: $\Delta\theta = 60 \text{ km s}^{-1}$ at $R = 4$ kpc, at which $\theta = 100 \text{ km s}^{-1}$ (Monnet, 1972).

5. "Optical-radio" Rotation Model (Fig. 3)

For the northern hemisphere we have used the $H\alpha$ results for $7 < R < 13$ kpc, and the Schmidt model for $R < 7$ kpc since the observed maximum $H 109\alpha$ velocity agrees with the maximum velocity predicted by the Schmidt model.

For the southern hemisphere we have used the $H\alpha$ results for $7 < R < 13$ kpc, and the maximum observed $H 109\alpha$ velocity for $3.9 < R < 5$ kpc. For $5 < R < 7$ kpc there are very few $H II$ regions and we cannot consider the observed maximum $H 109\alpha$ velocity as the velocity at the tangential point; thus for $5 < R < 7$ kpc we have interpolated the results of the two other sections of the rotation curve. It is clear that this section of the rotation curve is poorly defined but it has been used for the computation of only 11 kinematical distances of $H II$ regions.

The use of these separate northern and southern models has the two following advantages: it eliminates the 4 kpc "hole" near the tangential point at longitudes $\ell = 332^\circ$ and 337° , and it greatly improves the correlation between the kinematic and spectrophotometric distances, particularly for the $H II$ regions located between $\ell = 180^\circ$ and $\ell = 270^\circ$.

6. Calculation of the Kinematic Distances

In the rest of this article, for tracing the spiral structure we use the stellar distances whenever they are available. For optical and radio $H II$ regions for which spectrophotometric distances of the exciting star are not available, we have calculated the "kinematic" distances using the northern and southern rotation models. These kinematic distances and a comparison with the stellar distances have been discussed elsewhere (Georgelin, 1975).

IV. Identification and Correlation of Optical with Radio Data

1. Optical Results

Young clusters, exciting stars, and $H\alpha$ regions allow one to trace the spiral structure of our Galaxy in the solar neighborhood. We have published elsewhere (Crampton and Georgelin, 1975, Fig. 1) a study of the distribution of $H\alpha$ regions obtained from exciting star distances (based upon recent absolute magnitude calibrations) and from kinematic distances (based upon the rotation model of the $H II$ regions of § III). However, a discussion and a synthesis of these results in conjunction with those concerning the distribution of OB clusters—Becker and Fenkart (1971), Moffat and Vogt (1973)—and associations is necessary in order to disentangle the most important and best established spiral tracers. We shall show here, for a particular example, the type of study of detail that we have carried out for the entire Milky Way.

Associations, Young Clusters, Exciting Stars, and $H II$ Regions in the Perseus Arm

Figure 4a is a wide-field $H\alpha$ photograph of Dubout (1975). We have indicated in Fig. 4b, on the same scale, the positions of associations, clusters, and $H II$ regions. Examination of the positions, of the morphology, of the distances, and of the radial velocities shows that the Perseus arm is distinguishable from the local feature not only by distance (or radial velocity) but also by its position in the sky, as shown by the dashed line.

In Fig. 4 the local feature is at positive latitudes above the dashed line. The local feature is at a mean distance of 0.8 kpc; it includes three associations (Cep OB 2, Cep OB 3 and Cep OB 4), two clusters, and nineteen $H II$ regions detailed in Table 3.

In Fig. 4 the Perseus arm is at low negative latitudes below the dashed line. The Perseus arm is at a distance of 2.5 to 5 kpc; it includes ten associations (Cep OB 1, Cep OB 5, Cas OB 2, Cas OB 5, Cas OB 4, Cas OB 7, Cas OB 1, Cas OB 8, Per OB 1 and Cas OB 6), twenty-one clusters, and twenty-nine $H II$ regions detailed in Table 3. The boundary between these two groups permits, moreover, a more precise delimitation of the associations.

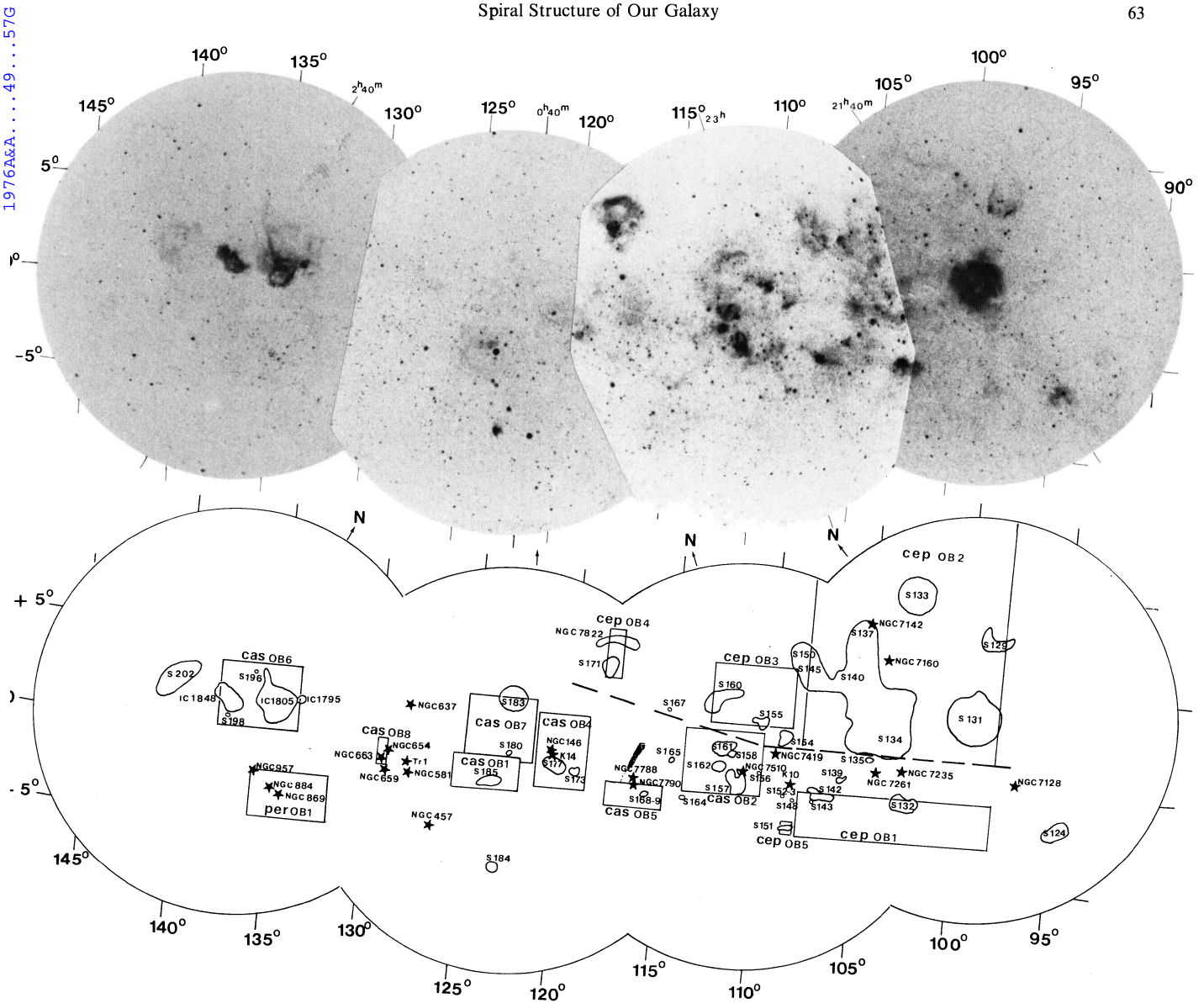


Fig. 4. (a) Monochromatic $H\alpha$ photographs of the Perseus arm between $\ell = 95^\circ$ and $\ell = 145^\circ$ (Dubout, 1975). (b) On the same scale, an identification chart of $H\text{ II}$ regions, stellar associations and OB clusters. Above the dashed line the local feature at positive latitudes and mean distance of 0.8 kpc. Below the dashed line the Perseus arm at low latitude and distance between 2.5 and 5 kpc

Note also that the dispersion in distance is greater for the second group (the Perseus arm), even allowing for the greater imprecision due to its distance. It appears that there are in fact many sub-groups at different distances in the interior of the Perseus arm. These sub-groups are:

a) From $\ell = 100^\circ$ to $\ell = 106^\circ$ the exciting stars and clusters have stellar distances between 3.1 and 4.1 kpc and latitudes between $-0^\circ6$ and $+0^\circ8$; this is therefore one sole group.

b) From $\ell = 106^\circ$ to $\ell = 123^\circ$ one can distinguish two subgroups by their distances:

— A sub-group at 2.5 kpc is comprised of the $H\text{ II}$ regions and clusters S 142 (NGC 7380), S 143, NGC 7510, S 157, S 161, S 162, S 163, S 164, S 165, S 168,

S 169, NGC 7788, NGC 7790, S 170, S 173, S 175, S 177, King 14, NGC 146, S 184.

— Another, at about 5 kpc, is more localised ($106^\circ < \ell < 112^\circ$ and $-3^\circ < b < +1^\circ$) and contains the two clusters NGC 7419 and King 10, and some small $H\text{ II}$ regions (S 151, 152, 153, 148, 149, 156, 158—for 148 and 149 we have only preliminary data for the exciting stars).

c) From $\ell = 124^\circ$ to $\ell = 133^\circ$ there are no $H\text{ II}$ regions, but seven clusters at distances between 2.1 and 2.8 kpc (NGC 457, NGC 581, Tr 1, NGC 637, NGC 654, NGC 659, NGC 663) which are in the extension of the first of the preceding sub-groups.

d) From $\ell = 133^\circ$ to $\ell = 138^\circ$ at 2.5 kpc, the associations Per OB 1 (h and χ Per) and Cas OB 6 (IC 1795, IC 1805,

Table 3

HII Region	Cluster	d (kpc)	V_{LSR} (km s ⁻¹)
a) Perseus arm			
	NGC 7128	3.1	
	NGC 7235	4.1	
S 132		3.6	- 50.9
	NGC 7261	3.2	
S 139		3.3	- 41.0
S 142	NGC 7380	2.4	- 35.8
S 143		3.7	- 28.8
	King 10	4.8	
S 151		5.1 k	- 54.9
S 152		3.4 k	- 44.3
S 153		4.0	- 52.8
	NGC 7419	6.0	
S 156		5.7	- 50.0
	NGC 7510	2.9	
S 157	An. Base 1 3	2.5	- 37.7
S 158		(4.3)	- 59.6
S 161		2.2	
S 162		3.5	- 45.2
S 163		2.3	- 42.6
S 164		3.1 k	- 44.0
S 165		1.6	- 27.5
S 168		3.0 k	- 43.5
S 169		1.5	
	NGC 7788	2.4	
	NGC 7790	3.2	
S 170		2.2	- 53.3
S 173		2.7	- 37.0
S 175		(1.7)	- 50.7
S 177		2.5	
	King 14	2.4	
	NGC 146	2.4	
S 184		2.2	- 27.8
	NGC 457	2.8	
	NGC 581	2.4	
	Tr 1	2.4	
	NGC 637	2.1	
	NGC 654	2.5	
	NGC 659	2.1	
	NGC 663	2.1	
IC 1795		2.3	- 40.7
S 190	IC 1805	2.3	- 46.0
	h Per	2.1	
	X Per	2.5	
	NGC 957	2.1	
S 196		3.6 k	- 43.0
S 198		2.8	- 33.5
S 199	IC 1848	2.3	- 36.6
b) Local feature			
S 125	IC 5146	1.0	+ 4.8
S 129		0.4	- 9.6
S 130 *			
S 131	IC 1396 (Tr 37)	0.9	- 2.2
S 133 *			
S 134		0.9	
	NGC 7160	0.7	
S 135		1.4	- 17.6
S 136 *			
	NGC 7142	0.6	
S 137		0.6	
S 140		0.9	- 10.0
S 144		0.1 k	- 1.7
S 145 *			
S 150 *			
S 154		1.0 k	- 11.4
S 155	Cep OB 3	0.7	- 15.1
S 160		0.8	
S 171	Cep OB 4	0.8	- 10.7

* S 130, S 133, S 136 have $b > 9^\circ$

S 145 and S 150 are in the same complex as S 140

IC 1848, S 196, S 198 and S 201—this last region having been studied by Dickinson *et al.*, 1974) continue the same alignment as the preceding associations.

2. H II Regions Observed Simultaneously in H α and H 109 α

Since the optical data and the radio data are complementary it is important to make sure that there is a fair amount of overlap between them. This requires that a sufficiently large number of H II regions be observed simultaneously by optical and radio means, and that the optical regions be observed out to fairly large distances.

Proportion of H 109 α Sources Detected Optically

Four hundred twenty H II regions are detected optically and 1300 H II regions are observed in the radio continuum. The radial velocities have been measured for 258 optical regions (H α) and for 212 radio regions (H 109 α or H 158 α). The optical and radio velocities are known simultaneously for only 58 of them, i.e., 22% of the measured optical regions and 27% of the radio regions. The radio observations are limited to the most intrinsically intense objects whereas the optical observations are mainly limited by absorption.

Optically, one can detect H II regions whose emission measures are 100 times weaker than the radio detection limit (Monnet, 1974). Hence even a weak radio region will be detected optically unless the absorption is greater than about five magnitudes.

Detection of Very Distant H II Regions

The optical detection of H II regions and of their exciting stars was formerly limited to a fairly small distance: about 3 kpc. In the past few years great optical progress has been made, on the one hand; and on the other hand the systematic search for H α regions and of hot stars in the vicinity of distant radio sources has led to the discovery of very distant H α regions.

Here are some examples of very distant H II regions detected optically:

a) The measurements of H α radial velocities and the distances of exciting stars have permitted us to detect, optically, very distant H II regions at $l = 291^\circ$. As Fig. 5 shows, one observed some nearby optical nebulae such as Gum 38 a (NGC 3576) and Gum 37 in this region, and the somewhat farther region RCW 55 with kinematic distance 5.7 kpc and stellar spectrophotometric distance 5.1 kpc (CPD -62° 1824). Figure 5 shows, especially, three very distant optical and radio regions: Gum 38b (NGC 3603) with an H α kinematic distance of 8.0 kpc, Gum 35 excited by Wolf-Rayet star LSS 2063 of stellar spectrophotometric distance 7.9 kpc, and the source 291.9-0.7 with an H α kinematic distance of 9.7 kpc. Thus there is a very good overlap between the

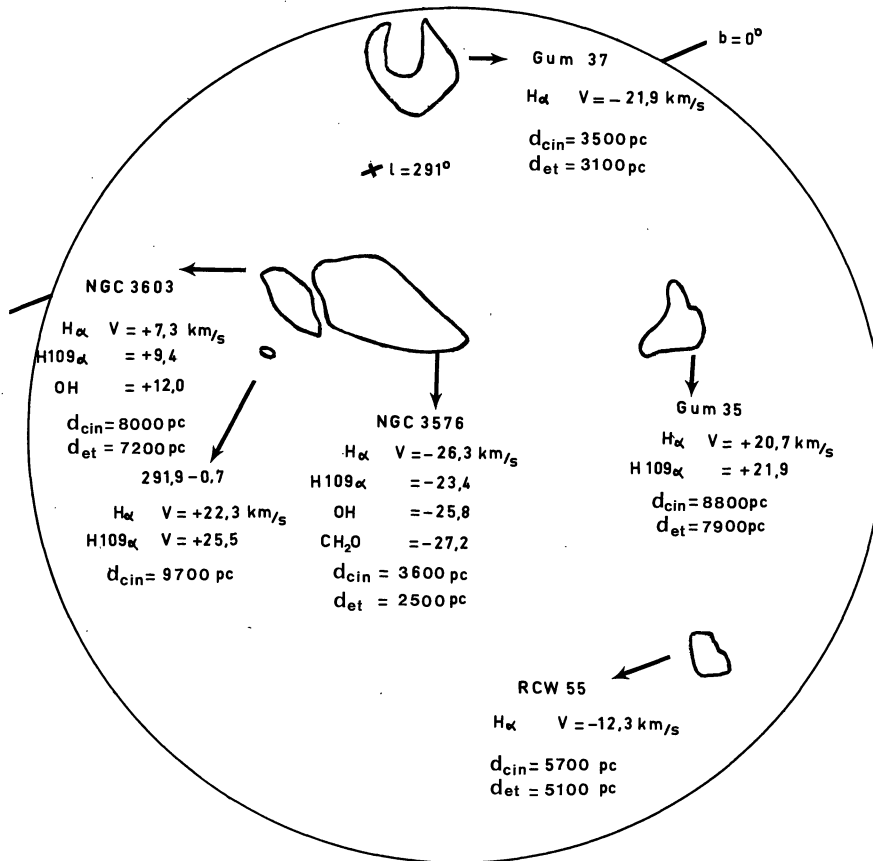


Fig. 5. Identification chart of $H\alpha$ regions near $\ell = 291^\circ$, showing radial velocities of $H\alpha$, $H 109\alpha$ and OH and CH_2O absorption components. Stellar distances and kinematic distances are indicated too

optical and radio data. Only the radio sources 298.8–0.3 and 298.9–0.4 at 11.7 kpc, and 289.1–0.4 at 8.9 kpc, are not observed optically.

b) $H\alpha$ photography (Georgelin and Georgelin, 1970a, Fig. 24, p. 29) shows a weak $H II$ region coinciding with the very distant radio source 316.8–0.1. This identification has been confirmed by Smith (1972). The observed radial velocities are given in Table 4. The mean velocity of -37 km s $^{-1}$ corresponds to distances of 2.1 and 12.5 kpc. The absorption profiles of Whiteoak and Gardner (1970) and Goss *et al.* (1972) show that this source is beyond the tangential point, i.e., at 12.5 kpc. The nebula observed optically at this location seems therefore the farthest known to date, and it would be interesting to be able to detect its exciting star.

c) Recently we have optically detected three $H II$ regions in W 51 with $H\alpha$ monochromatic photographs, the first $H\alpha$ region corresponding to 49.0–0.3 and the two others to 49.5–0.4. From Fabry-Perot rings we have measured their radial velocities which agree with the $H 109\alpha$ radial velocities. These results will be published later with more details (Georgelin, 1976).

d) We note also, among the very distant optical groups, the complex of $H II$ regions at 8.8 kpc and at $\ell = 70^\circ$. This radio complex W 58 contains three $H\alpha$ regions cited by Minkowski (1946): Mi I.18 (NGC 6857=S 100),

Table 4. Radial velocities of 316.8–0.1

Component	V_{LSR} (km s $^{-1}$)	Reference
$H 109\alpha$	-36.1	Wilson <i>et al.</i> (1970)
OH absorption	-38.0	Robinson <i>et al.</i> (1971)
CH_2O	-37.7	Whiteoak and Gardner (1970)
	-41.8	
	-45.6	
	-45.6	
$H I$ absorption	-38.1	Goss <i>et al.</i> (1972)
	-45.4	
	-52.9	

Mi I.16 (S 99) and Mi I.17 (70.4+1.6); these three regions are within a more extended $H\alpha$ region which has since been observed in the radio continuum by Israel (1974). We have found (Georgelin *et al.*, 1973) that the radial velocities of the three $H\alpha$ regions and of the surrounding region are the same, which shows that this is indeed a complex of regions at the kinematic distance of 8.7 kpc. The distance of the exciting star of NGC 6857 confirms this distance.

To the south of W 58 Dickel and Milne (1972) have detected, in $H 109\alpha$, a new $H II$ region—69.9+1.5— with a radial velocity of -61 km s $^{-1}$. Recently, in $H\alpha$, we have measured the radial velocity of 69.9+1.5 as $V_{LSR} = -35$ km s $^{-1}$. This result shows that 69.9+1.5

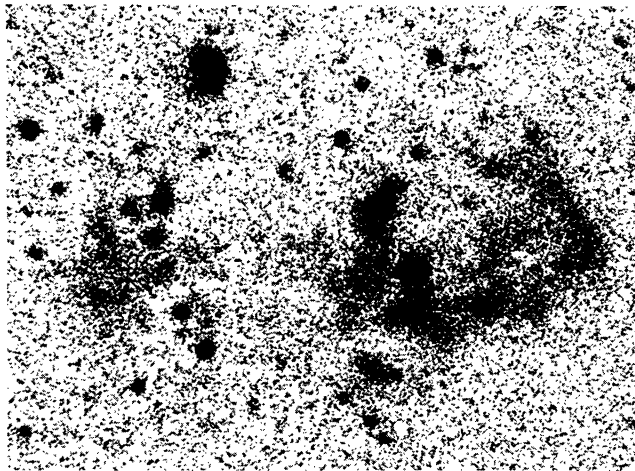
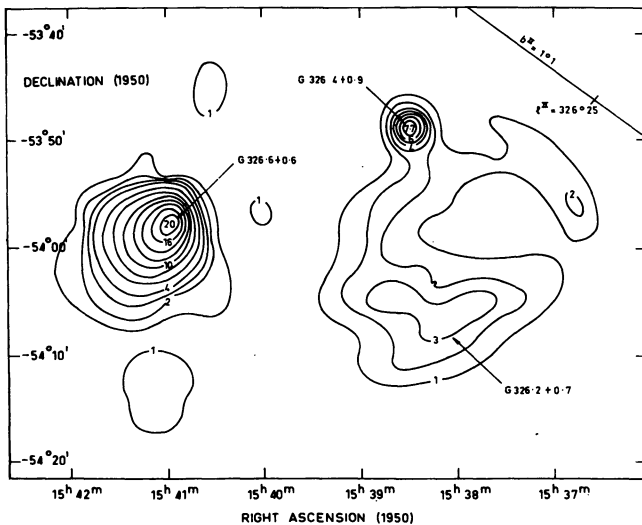


Fig. 6. (a) Radio continuum map of Shaver and Goss (1970). (b) On the same scale, $H\alpha$ photograph of the optical sources RCW 94, RCW 95 and 326.6+0.6

lies either at 8.8 kpc (the distance of W 58), or at 9.5 kpc ($V_{\text{LSR}} = -35 \text{ km s}^{-1}$) which put it in the same spiral arm that W 58.

At the neighboring longitude $l = 79^\circ$ is the $H 109\alpha$ source 79.3+1.3 (DR 7). Reifenstein *et al.* (1970) have calculated the kinematic distance of this source (8.0 kpc) which certainly is a part of the same spiral arm as W 58 but is not detected optically.

e) Around the same longitudes, several optical and radio regions are located at distances of about 5 kpc, e.g., S 104 at $l = 74^\circ 8'$ and distance 4.8 kpc, with matching $H\alpha$ and $H 109\alpha$ velocities (Dickel and Milne, 1972); and the peculiar nebula S 106 at about 5.8 kpc, which shows strong expansion velocities (Maucherat, 1975).

Thus there now is a good overlap between the optical and radio data, which facilitates the interpretation of the radio results and permits the determination of a unique rotation model from $H\alpha$ and $H 109\alpha$ velocities and stellar distances.

3. Optical Identification of Radio Sources

To trace the spiral structure of our Galaxy, it is indispensable to harmonize and to clarify all of the observational results. For a single well-defined $H II$ region we can have the spectrophotometric distance of the exciting star, the $H\alpha$ kinematic distance, and the $H 109\alpha$ kinematic distance (s) (near and far): of course we have compared these results in order to obtain only one distance for this region (examples § IV 2, 3). For a complex of $H II$ regions, when there was convincing evidence ($H\alpha$ photograph, radio continuum map, morphology, matching radial velocities or distances, etc.) that the various features do belong together we have assigned a unique distance to this complex (examples § IV 3, V). For the whole Milky Way we have thus made optical identifications of these $H 109\alpha$ sources, especially by using $H\alpha$ photographs of $H II$ regions (Georgelin and Georgelin, 1970a), and radio continuum maps (Shaver and Goss, 1970).

We present below three examples of this analysis, for $l = 326^\circ$, $l = 328^\circ$ and $l = 291^\circ$.

a) $H II$ Regions at $l = 326^\circ$

An $H\alpha$ photograph (Georgelin and Georgelin, 1970a) shows two previously known $H II$ regions, RCW 94 and RCW 95, and two new $H II$ regions that we have detected. These four nebulae are connected by very weak emission. The optical radial velocities $C - 43.8$, -38.6 , -41.3 and -39.5 km s^{-1} confirms the physical connection.

The continuum radio map of Shaver and Goss (1970), reproduced in Fig. 6 along with an enlargement, at the same scale, of part of the $H\alpha$ photograph, shows that the radio source 326.5+0.9, also detected in $H 109\alpha$, is associated with the optical nebula RCW 94. The radio contours correspond rather well with the optical form, particularly in the south and in the west. The radial velocities are -41.3 and -39.0 km s^{-1} in $H\alpha$ and in $H 109\alpha$, respectively.

The same continuum map shows also that the radio source 326.6+0.6 coincides with one of the two new nebulae discovered in this photograph and not with RCW 95. The observed radial velocities are given in Table 5.

We therefore conclude that there is a single complex of $H II$ regions comprising four optical nebulae, of which two were detected by radio ($H 109\alpha$, OH and CH_2O). The mean of the $H\alpha$ and $H 109\alpha$ observed velocities, -40.6 km s^{-1} , gives the kinematic distance—2.5 kpc—of this unique complex.

b) $H II$ Regions at $l = 328^\circ$

The $H\alpha$ photograph of this field (Georgelin and Georgelin, 1970a, Fig. 32, p. 37) shows an annular region of diameter 3° with a number of condensations including RCW 96, RCW 97, RCW 98, RCW 99 and 328.1-0.5.

The association of these various nebulae with the extended region is confirmed by their radial velocities which are, respectively, -51.5 , -49.2 , -40.1 , -47.8 , -42.0 and -47.7 km s^{-1} .

The radio continuum map of Shaver and Goss (1970) shows that the nebula RCW 97 coincides with an extension towards the southwest of the radio source 327.3–0.5. The various radial velocities are in excellent accord, as can be seen from Table 6.

The radio source 328.0–0.6 is close to the optical region 328.1–0.5. The radial velocities agree: -42.0 km s^{-1} for $\text{H}\alpha$ (Georgelin, 1975) and -42.9 km s^{-1} for $\text{H 109}\alpha$ (Caswell, 1972).

The radio source 328.0–0.1, observed in $\text{H 109}\alpha$, has no optical counterpart but its velocity of -44.7 km s^{-1} agrees well with that of this complex with which it certainly is associated.

We therefore conclude that, morphologically and kinematically, all these regions form a single complex of mean radial velocity -46.2 km s^{-1} , corresponding to a kinematic distance of 2.9 kpc. This is in agreement with the distance of the exciting stars—2.6 kpc—and with the concentrations of OB stars at 2.5 kpc observed by Muzzio and McCarthy (1973).

c) H II Regions at $\ell = 291^\circ$

The $\text{H}\alpha$ and $\text{H 109}\alpha$ velocities, as well as the velocities for diverse molecules observed in absorption, are indicated in Fig. 5 for each H II region. For each region the agreement between the various velocities is excellent, and therefore we are sure that these H II regions are at different distances. In addition, these kinematic distances, ranging from 2.5 kpc to 9.5 kpc, agree with the independently determined stellar distances (Georgelin and Georgelin, 1970). This is therefore a good example of convergence between all of the optical and radio data; it shows the spread in distance of the Carina arm which is aligned along the line of sight at this longitude.

We have made these identifications and correlations between all of the optical and radio results for the galactic plane in order to have homogeneous observational material available for the tracing of the spiral structure.

V. Regions at Longitudes 332° and 337°

This zone of longitude is crucial¹⁾ for tracing the spiral structure. For one thing, the line of sight intersects the spiral arms out to great distances and over the entire range of galactocentric distance from 4 kpc to 12 kpc; also the differential rotation is large and there is there-

¹⁾ The symmetrical region at $\ell = 23^\circ$ – 28° is less crucial, because for trailing spirals, we intersect—at near distance, $r < 10$ kpc—more spiral arms and in a more perpendicular way at $\ell = 330^\circ$ than at $\ell = 30^\circ$.

Table 5. Radial velocities of 326.6+0.6

Component	V_{LSR} (km s^{-1})	Reference
$\text{H}\alpha$	-43.8	Georgelin (1975)
$\text{H 109}\alpha$	-44.5	Wilson <i>et al.</i> (1970)
OH absorption	-44.1	Goss <i>et al.</i> (1970)
	-21.2	
	-45	
CH_2O	-21	Robinson <i>et al.</i> (1971)
	-43.6	
	-22.2	
		Whiteoak and Gardner (1970)

Table 6. Radial velocities of 327.3–0.5

Component	V_{LSR} (km s^{-1})	Reference
$\text{H}\alpha$	-49.2	Georgelin and Georgelin (1970)
$\text{H 109}\alpha$	-48.8	Wilson <i>et al.</i> (1970)
H I absorption	-49.5	Goss <i>et al.</i> (1972)
OH absorption	-49.0	Robinson <i>et al.</i> (1971)
CH_2O	-50.8	Whiteoak and Gardner (1970)

fore a wide spread of radial velocities, allowing one to discriminate between various velocity groups—i.e., spiral arms. Observation of H II regions at $\text{H 109}\alpha$ is very fruitful since fifteen and seventeen regions are detected at $\ell = 332^\circ$ and 337° respectively. Clearly, a general interpretation of the spiral structure of our Galaxy first requires a satisfactory interpretation of these thirty-two regions (which have 64 possible kinematic distances).

1. H 109 α Regions at $\ell = 332^\circ$

Between $\ell = 330^\circ.9$ and $\ell = 333^\circ.7$ are fifteen $\text{H 109}\alpha$ regions, whose velocities range from -47.0 km s^{-1} to -90.8 km s^{-1} . When we plot the kinematic distances this gives thirty possible points along the line of sight. We have already seen that a number of $\text{H 109}\alpha$ sources thus detected may be the intensity maxima of a single region; this is particularly true here, in this field which is very rich in H II regions (as well as hot stars), as is shown in the $\text{H}\alpha$ photograph on which are also indicated the $\text{H 109}\alpha$ sources (Georgelin, 1970, Fig. 2, p. 325).

Precise optical identification shows that

- the two $\text{H 109}\alpha$ sources—332.7–0.6 and 332.8–0.6, with velocities of -47.0 km s^{-1} and -57.2 km s^{-1} respectively—correspond exactly to two optical zones of similar velocity in the same H II region, RCW 106 (-47.0 and -58.3 km s^{-1} respectively);
- the two $\text{H 109}\alpha$ sources 333.0–0.4 and 333.1–0.4, with velocities of -53.8 and -55.8 km s^{-1} , situated on the edge of the optical H II region 333.1–0.6 and having the same radial velocity, correspond to this same single H II region which is, moreover, at the same distance as RCW 106; and
- similarly, the sources 332.2–0.5 and 333.3–0.4, of velocities -55.0 and -50.1 km s^{-1} , have weaker optical

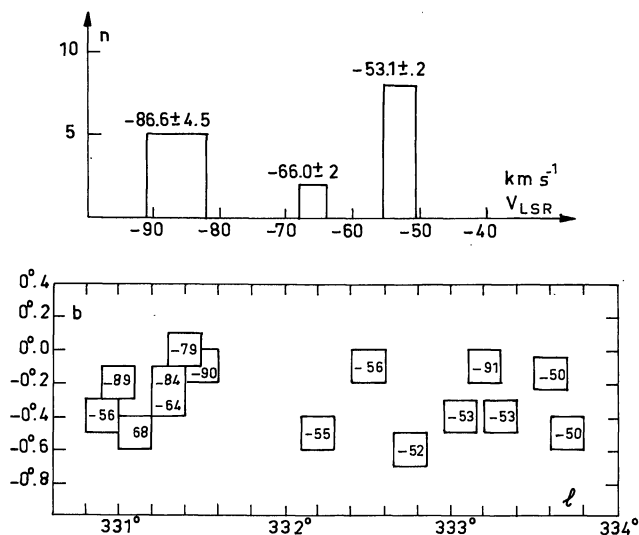


Fig. 7. (a) H 109α radial velocities of fifteen sources near $\ell=332^\circ$. Histogram of the number of sources as a function of radial velocity. (b) Grouping of these fifteen H 109α sources as a function of longitude and latitude

and $-86 \pm 4.5 \text{ km s}^{-1}$ which correspond to three different distances. Figure 7b shows the positions of these regions in the sky (ℓ, b), along with their velocities. We note that:

- The five sources (group 1) with the greatest velocities (-86.6 km s^{-1}) are concentrated at very low latitudes ($-0^\circ 2 < b < 0^\circ$). None of them is detected optically. Their distance is 7.8 or 9.7 kpc.
- The eight H 109α sources (group 3) of velocities -50 to -56 km s^{-1} constitute a single “near” complex (4.2 kpc) of which a large part is detected optically (six H II regions and numerous OB stars).
- The two H 109α sources (group 2) of velocities -64 and -68 km s^{-1} are closely neighboring H II regions and constitute an optically non-detected group which cannot be integrated with the two preceding groups.

2. H 109α Regions at $\ell=337^\circ$

Between $\ell=335^\circ 8$ and $\ell=338^\circ 4$ are seventeen H 109α regions of velocities between -4 and -93 km s^{-1} .

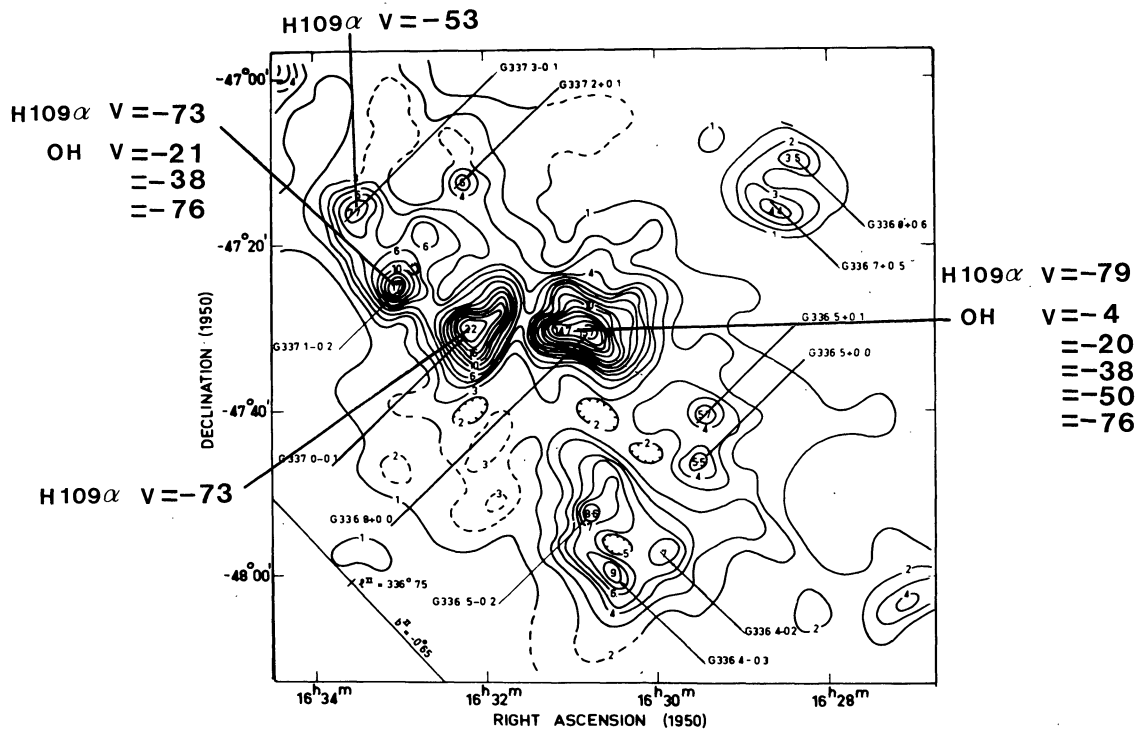


Fig. 8. 408 MHz continuum maps of Shaver and Goss (1970) at longitude 336° . Radial velocities (in km s^{-1}) of group 4 (No. 89 in Table 9)

counterparts. We may conclude that these six H 109α sources are certainly part of the same complex as the six optical H II regions of this field.

We have grouped $332.7-0.6$ with $332.8-0.6$, $333.0-0.4$ with $333.1-0.4$, and $333.6-0.1$ with $333.6-0.2$. We have taken the mean of the radial velocities from H α and H 109α , in agreement with other constituents (three CH₂O sources, two H₂O sources and one OH absorption region). In Fig. 7a the mean velocities are assembled in three groups centered on -53 ± 2 , -66 ± 2

The optical H II regions identified in this sector of longitude are:

- RCW 107, comprised of the two small symmetric nebulae NGC 6164 and NGC 6165 which are in expansion around the Of star HD 148937. This nebula has been studied in detail by Fabry-Perot interferometry by Pismis (1974). The identification of NGC 6164 with the H 109α source 336.4-0.2 is sure; the identification of NGC 6165 with 336.4-0.3 is a little less sure but the distance of 7.3 s of arc between the two radio sources

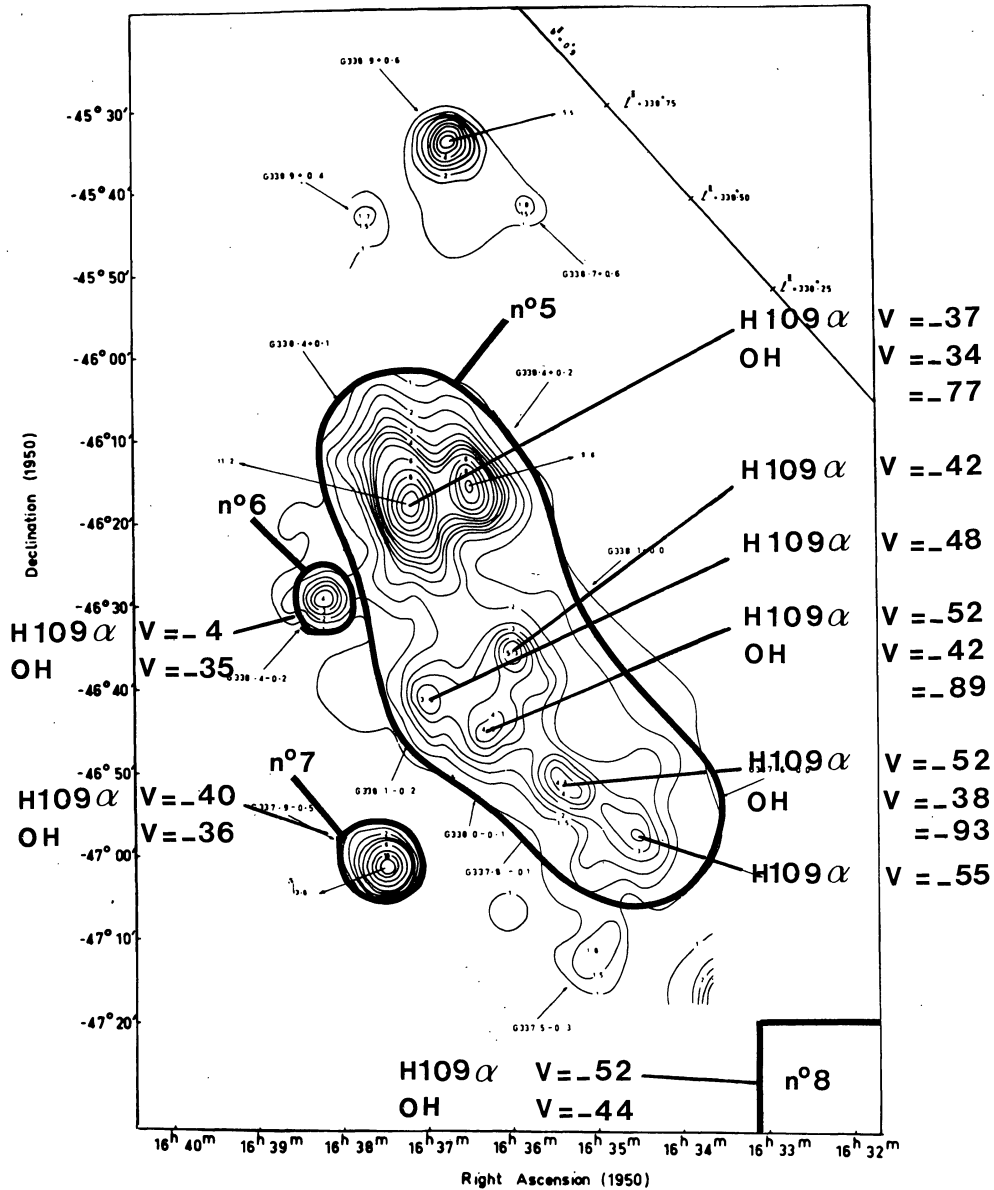


Fig. 9. 5000 MHz continuum maps of Shaver and Goss (1970) at longitude 338°. Identifications and radial velocities (in km s^{-1}) of groups 5, 6, 7 and 8 (Nos. 91, 92, 90 and 87 in Table 9)

coincides well with the distance between the two principal optical condensations, although the orientation is slightly different. These two radio sources have radial velocities of -68 and -93 km s^{-1} respectively, with a greater than normal "turbulence". Optically too, one observes (Pismis, 1974) very large internal motions—from $+20 \text{ km s}^{-1}$ to -120 km s^{-1} —with mean velocities of -20 and -80 km s^{-1} for the two condensations. Analysis of the radio continuum map of Shaver and Goss (1970) shown in Fig. 8 suggests that the two other closely neighboring sources, $336.5+0.0$ and $336.5-0.2$, with similar radial velocities (-63 and -88 km s^{-1} respectively), should be grouped with this very peculiar complex which we shall not use for tracing the spiral structure.

— RCW 108, a very large (diameter 3°) and brilliant optical H II region of mean velocity -19.9 km s^{-1} which corresponds to a single H 109α source, $336.5-1.5$, of velocity -24.9 km s^{-1} (group 9).

Analysis of the radio continuum maps of Shaver and Goss (1970) reproduced in Figs. 8 and 9 shows that:

— The three sources $336.8+0.0$, $336.9-0.1$ and $337.1-0.2$ constitute a single complex (group 4, Fig. 8), which is confirmed by the H 109α velocities, respectively -78.9 , -73.1 and $-72.7 \pm 1.8 \text{ km s}^{-1}$.

The clearly weaker source $337.3-0.1$ seems linked to this complex in spite of a different, but more uncertain, radial velocity: $-53.5 \pm 6.6 \text{ km s}^{-1}$. From this complex's mean velocity we obtain a distance of 11.7 or 6.7 kpc.

— The neighboring sources $337.6-0.0$, $337.8-0.1$,

Table 7. H II Region Complexes at $\ell = 332^\circ$ and $\ell = 337^\circ$

Group	ℓ	Mean V_{LSR} (km s^{-1})	Number of regions	Distances (kpc)	Numero (Table 9)
1	331 $^\circ$ 7	-86.6	5	7.8 or 9.8	85
2	331 $^\circ$ 2	-66.0	2	5.4 or 12.1	84
3	332 $^\circ$	-53.1	8	4.2 or 13.4	86
4	336 $^\circ$ 9	-74.9	3	6.7 or 11.7	89
5	338 $^\circ$	-46.9	5	4.4 or 14.1	91
6	338 $^\circ$ 4	-4.3	1	0.6 or 18.0	92
7	337 $^\circ$ 9	-40.4	1	3.7 or 14.8	90
8	335 $^\circ$ 8	-52.1	1	4.6 or 13.7	87
9	336 $^\circ$ 5	-19.9	1	1.3	88

Table 8. Observed and calculated radial velocities

Velocities observed at 332 $^\circ$ (groups 1 and 2)	-88.6 km s^{-1} (group 1)	-66.0 km s^{-1} (group 2)
Predicted velocities at 337 $^\circ$ assuming circular arms	-71.7 (group 1)	-51.9 (group 2)
Predicted velocities at 337 $^\circ$ assuming spiral arms inclined at 12 $^\circ$, for the case of near solution	-77.7 (group 1)	-53.9 (group 2)
Predicted velocities at 337 $^\circ$ assuming spiral arms inclined at 12 $^\circ$, for the case of the distant solution	-63.6 (group 1)	-46.3 (group 2)
Velocities observed at 337 $^\circ$ (groups 4 and 5)	-74.9 (group 4)	-46.9 (group 5)

338.1-0.2 and 338.1+0.0 are connected together and to the two intense sources 338.4+0.2 and 338.4+0.1; they constitute a complex (group 5, Fig. 9) spread out along the galactic plane. The H 109 α velocities (-54.8, -52, -52.5, -47.7, -41.7 and -38 km s^{-1}) are in agreement, and the mean velocity of -46.9 km s^{-1} gives a distance of 4.4 or 14.1 kpc for this complex.

— The source 338.4-0.2 (group 6, Fig. 9) is not really part of the complex; this is confirmed by a very different velocity—-4.3 km s^{-1} —corresponding to a distance of 0.6 or 18.0 kpc.

— The two sources 335.8-0.2 (group 8, Fig. 9) and 337.9-0.5 (group 7, Fig. 9) are not connected with the preceding complexes.

3. Interpretation

After examining the various optical and radio data, the thirty-two H 109 α regions were separated into the nine groups of Table 7.

We have seen in Fig. 7 that at longitude 332 $^\circ$, groups 1, 2 and 3 have velocities of -86.6, -66.0 and -53.1 km s^{-1} . By simple continuity of the spiral arms one should find these same velocities slightly shifted at a nearby longitudes. The predicted velocities of these regions at longitude 337 $^\circ$ are given in Table 8.

This table shows:

- that there is velocity continuity between groups 1 and 4,
- that there is velocity continuity between groups 2 and 5,
- that the continuity between 1 and 4 is much better in the case of the “near” distance,
- that the continuity between 2 and 5 is much better in the case of the “far” distance.

Choice of Distances (Fig. 10)

Group 3 (No. 86). Six of the eight sources of group 3 are detected optically and are situated at 4.2 kpc. The sources detected in absorption have no higher velocity component. There is no doubt concerning the “near” distance for group 3.

Group 9 (No. 88). Group 9 is identified with RCW 108, which is part of the Sagittarius-Carina arm.

Group 5 (No. 91). For group 5 there is no question that the distance solution at 14.1 kpc is correct, because there are three OH sources and one H I component in absorption at greater absolute velocities (-77, -89, -93 and -60 km s^{-1}). The very low latitude (0 $^\circ$ 0, 0 $^\circ$ 0, -0 $^\circ$ 1 and -0 $^\circ$ 2), and the shape of the complex, spread out along the galactic plane, does not contradict this hypothesis.

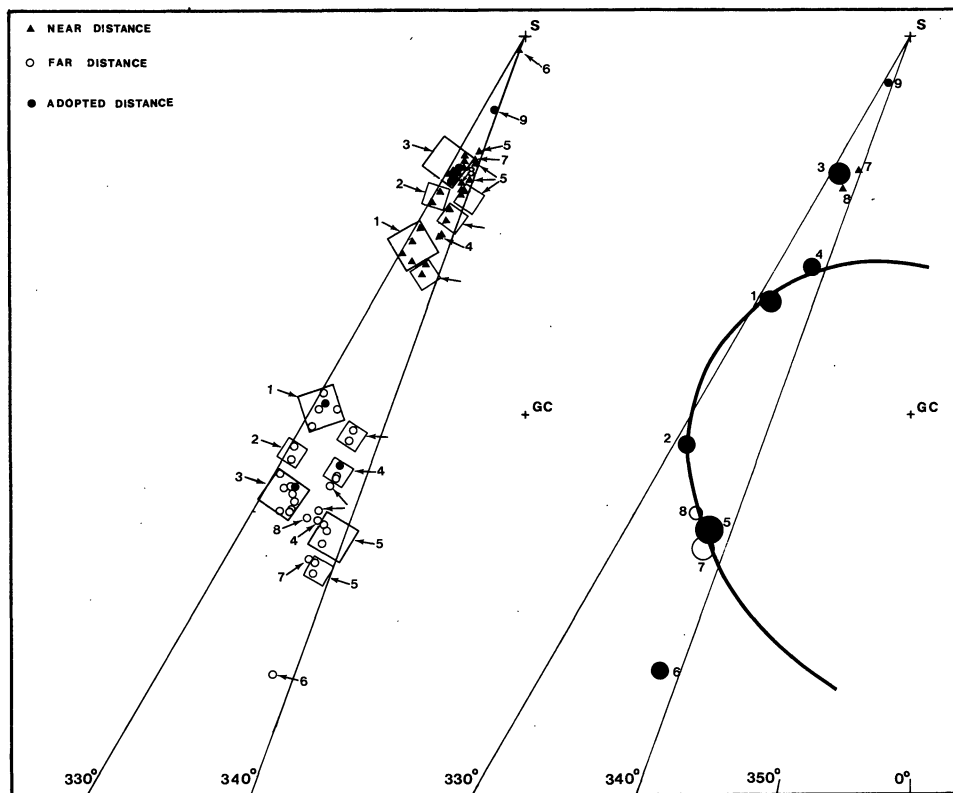


Fig. 10. Grouping and interpretation of the thirty-two H 109 α regions between $\ell = 330^\circ$ and $\ell = 340^\circ$

Group 6 (No. 92). If group 6 were at 0.6 kpc it would be detected optically. In addition, Caswell and Robinson (1974) have found OH in absorption at -35 km s^{-1} . The “far” distance at 18 kpc is therefore adopted.

Group 4 (No. 89). In front of two of the sources of group 4, Caswell and Robinson (1974) have detected OH in absorption, but none of the radial velocity components is more negative than that of H 109 α , even though OH absorption components with radial velocities up to the subcentral velocity have been observed at the same longitude (e.g., in front of group 5). Thus group 4 is at the “near” distance.

Group 2 (No. 84). We have already seen that group 2 is associated (Table 8) with group 5, which is distant. Therefore we chose the distant solution for group 2.

Group 1 (No. 85). There is a continuity of velocity between group 1 and the “near” group 4. Furthermore, the hypothesis of the “near” solution places these two groups on the same spiral as groups 2 and 5.

Groups 7 and 8 (Nos. 90 and 87). For groups 7 and 8 the choice is difficult. We adopt the “near” distance without strong conviction; OH absorption components have been detected (Caswell and Robinson, 1974) but the H 109 α velocity is slightly offset from the OH velocities.

Figure 10 groups the results of all the § V.

We have made the same discussion for each complex in the whole galactic plane.

In Table 9 we give the data: running number, mean longitude, adopted V_{LSR} , spectrophotometric or kinematic distance, excitation parameter (see § VI, 1) and exciting stars for each complex with $U > 70 \text{ pc cm}^{-2}$; H 109 α and H α identification and their V_{LSR} for each component.

In Table 10 we give the criteria used (§ II, 4) to resolve distance ambiguity for each complex.

VI. Outline of the Large-Scale Spiral Structure

1. Description of the Ionized Hydrogen Spirals Arms (Fig. 11)

Figure 11 has been made from the pertinent data (longitude, radial velocity, spectrophotometric or kinematic distance, choice of “near” or “far” distance) obtained for each complex of H II region. Details are in Tables 9 and 10.

In Fig. 11 we show only the “important” H II regions²⁾ ($U > 70 \text{ pc cm}^{-2}$), and we have “weighted” each of them according to its excitation parameter U : bright (b) for $U > 200 \text{ pc cm}^{-2}$, medium (m) for $110 < U < 200 \text{ pc cm}^{-2}$, faint (f) for $70 < U < 110 \text{ pc cm}^{-2}$. The main effect of this weighting is to show the relative insignificance of our local region of the Galaxy, which does not

²⁾ The “giant” H II regions of Mezger (1970) are defined by $\delta D^2 > 400 \text{ f.u. kpc}^2$, corresponding to $U > 100 \text{ pc cm}^{-2}$.

Table 9

No	l	adopted V_{LSR} (km s $^{-1}$)	d_{star} (kpc)	d_{kin} (kpc)	U (pc cm $^{-1}$)	H109 α source	H α source	V_{LSR} H109 α (km s $^{-1}$)	V_{LSR} H α (km s $^{-1}$)
1	6 $^{\circ}$ 0	+ 4.4	1.5		ϵ	6.0 - 1.2	M 8	+ 3.0	+ 5.7
cluster NGC 6530									
2	7 $^{\circ}$ 0	+13.8	2.7		ϵ	7.0 - 0.2	M 20	+16.4	+11.3
HD 164492									
3	8 $^{\circ}$ 5	+35	5.3		ϵ	8.5 - 0.3		+35	
4	10 $^{\circ}$ 3	+ 8.0	18.7	b		10.2 - 0.3 10.3 - 0.1 10.6 - 0.4		+13.9 + 9.7 + 0.3	
5	12 $^{\circ}$ 8	+36.3	4.2	m		12.8 - 0.2		+36.3	
6	13 $^{\circ}$ 2	+57.0	5.8	ϵ		13.2 + 0.0		+57.0	
7	14 $^{\circ}$ 6	+37.2	4.0	ϵ		14.6 + 0.1		+37.2	
8	15 $^{\circ}$ 1	+18.1	2.5	m		15.1 - 0.7	M 17	+17.2	+19.0
cluster NGC 6618									
9	17 $^{\circ}$ 0	+26.4	2.0	ϵ		17.0 + 0.8	M 16	+24.5	+28.4
cluster NGC 6611									
10	18 $^{\circ}$ 2	+47.4	4.3	ϵ			S 53		+47.4
11	18 $^{\circ}$ 6	+31.1	2.2	m		18.5 + 1.9	S 54	+32.9	+29.4
BD -11 $^{\circ}$ 4581 BD -12 $^{\circ}$ 4964 BD -12 $^{\circ}$ 4970 BD -12 $^{\circ}$ 4973 BD -12 $^{\circ}$ 4975 BD -12 $^{\circ}$ 4979 BD 167971 BD -12 $^{\circ}$ 4982 BD -12 $^{\circ}$ 4984 BD 168112 BD -12 $^{\circ}$ 4994 BD 168206									
12	19 $^{\circ}$ 1	+67.3	13.4	m		19.1 - 0.3		+67.3	
13	19 $^{\circ}$ 7	+43.4	3.8	ϵ		19.7 - 0.2		+43.4	
14	20 $^{\circ}$ 7	+57.4	14.0	m		20.7 - 0.1		+57.4	
15	22 $^{\circ}$ 8	+82.5	12.4	b		22.8 - 0.3		+82.5	
16	23 $^{\circ}$ 4	+101.5	7.3	m		23.4 - 0.2		+101.5	
17	24 $^{\circ}$ 6	+113.1	9.1	m		24.6 - 0.2 24.5 + 0.2 24.8 + 0.1		+109.2 +116.0 +114.1	
18	25 $^{\circ}$ 4	+ 60.4	13.6	b		25.4 - 0.2		+ 60.4	
19	25 $^{\circ}$ 8	+110.0	9.0	m		25.8 + 0.2		+110.0	
20	28 $^{\circ}$ 0	+ 96.9	6.9	m		*27.3 - 0.2 28.6 + 0.0		+ 97.6 + 96.2	
21	29 $^{\circ}$ 9	+ 96.4	7.0	m		29.9 - 0.0 (30.2 - 0.2)		+ 96.4 (+101.0)	
22	30 $^{\circ}$ 8	+ 92.5	6.6	b		30.8 - 0.0 (31.1 + 0.0)		+ 92.5 (+ 99.2)	
23	34 $^{\circ}$ 3	+ 53.9	3.6	ϵ		34.3 + 0.1		+ 53.9	
24	35 $^{\circ}$ 2	+ 46.5	3.0	ϵ		35.2 - 1.7		+ 46.5	
25	36 $^{\circ}$ 4	+ 57.4	3.9	ϵ			S 72	+ 57.4	
26	37 $^{\circ}$ 6	+ 51.8	12.4	b		37.4 - 0.2 37.6 - 0.1 37.9 - 0.4		+ 39.0 + 55.8 { + 60.2 + 61.0	
27	43 $^{\circ}$ 2	+ 8.6	14.1	b		43.2 - 0.0		+ 8.6	
28	45 $^{\circ}$ 5	+ 55.5	3.9	ϵ				45.5 + 0.0 45.5 + 0.1	+ 57.4 { + 53.0 + 54.0
29	48 $^{\circ}$ 6	+ 17.0	11.9	m		48.6 + 0.0			+ 17.0
30	49 $^{\circ}$ 2	+63.5	5.8	b		48.9 - 0.3 49.0 - 0.3 49.1 - 0.4 49.2 - 0.3 49.4 - 0.3 49.5 - 0.4		[49.0 - 0.3] [49.5 - 0.4]	+66.4 { +63.2 +65.8 +72.4 { +66.1 +67.2 +52.8 { +59.0 +58.2
31	49 $^{\circ}$ 3	+52.6	4.4	m		51.2 - 0.1 51.4 - 0.0			+55.3 +49.8
32	70 $^{\circ}$ 3	-23.4	8.8	b		70.3 + 1.6 70.3 + 1.6	NGC6857-8100 K 3.50 S 99	-24.4 -24.2	-21.7 -22.0 -24.4 (-35)
An. $\alpha_{1950} = 19^{\text{h}}39^{\text{m}}9.6$, $\delta_{1950} = 33^{\circ}23'$ (Liller and Chang Yuan Shao, 1968 Crampton and Georgelin, 1975)									
33	75 $^{\circ}$ 8	- 4.8	5.7	ϵ		75.8 + 0.4			- 4.8
34	76 $^{\circ}$ 4	- 7.6	5.8	ϵ		76.4 - 0.6	S 106		+ 5.6 - 7.6
35	79 $^{\circ}$ 3	-41.4	7.6	m		79.3 + 1.3			-41.4
36	79 $^{\circ}$ 9	-18.7	5.7	m		79.8 + 1.2 80.0 + 1.5			-22 -15.4
37	80 $^{\circ}$ 0	(x)	1.4	m		Cygnus X complex	S 109		
38	84 $^{\circ}$ 9	+ 2.1	2.0	ϵ			S 115		+ 2.1
BD 46 $^{\circ}$ 2972 BD 46 $^{\circ}$ 2978 LSIII 46 $^{\circ}$ 11 LSIII 46 $^{\circ}$ 12									
39	85 $^{\circ}$ 5	+ 3.0	0.8	ϵ		84.9 - 0.7 (158 μ) (166 μ)	NGC7000-8117	- 0.4 + 4.2	+ 3.0
HD 199579									
40	102 $^{\circ}$ 8	-50.9	3.6	m			S 132		-50.9
LSIII 55 $^{\circ}$ 32 HD 211853 BD 55 $^{\circ}$ 2722									
(x) The kinematic distances have little significance for Cygnus X sources.									
41	111 $^{\circ}$ 3	-37.7	2.5	ϵ			S 157		-37.7
HD 219286 BD 55 $^{\circ}$ 2677 LSIII 55 $^{\circ}$ 57 HD 219460 LSIII 55 $^{\circ}$ 66 Cluster An. Rosal 3									
42	111 $^{\circ}$ 5	-60.1	2.8 (5.8)	m			S 158	-60.6	-59.6
Astrographic Cat. Vatican n $^{\circ}$ 37622 An. at 1' in SW									
43	133 $^{\circ}$ 7	-42.7	2.3	m		133.7 + 1.2 134.8 + 1.0	IC 1795 IC 1805	-42.3 -41.7	-40.7 -46.0
BD 61 $^{\circ}$ 411 Cluster IC 1805									
44	137 $^{\circ}$ 5	-36.6	2.3	ϵ		137.3 + 1.0	IC 1848	-37.0	-36.6
Cluster IC 1848									
45	150 $^{\circ}$ 6	-23.0	3.6	ϵ		150.6 - 0.9	S 206	-22.0	-24.0
BD 50 $^{\circ}$ 886									
46	151 $^{\circ}$ 6	-46.6	> 4.8	ϵ		151.6 - 0.2	S 209	-46.1	-47.1
47	173 $^{\circ}$ 5	- 0.9	3.4	m		173.4 - 1.8	IC 410	- 1.8	+ 0.0
Cluster NGC 1893									
48	206 $^{\circ}$ 3	+19.6	1.5	ϵ		206.4 - 1.9	S 275	+17.8	+21.5
Cluster NGC 2244									
49	209 $^{\circ}$ 0	+ 3.2	0.4	ϵ		206.5 - 16.4 208.9 - 19.3 209.0 - 19.4	NGC 2024 NGC 1976	{ + 7.0 { + 6.0 + 7.7 - 2.8	{ - 3.5 { + 8.7 + 1.2
Association Ori OB1									
50	227 $^{\circ}$ 7	+56.3	5.2	ϵ			S 298		+56.3
HD 56925									
51	243 $^{\circ}$ 3	+46.6	4.1	ϵ		243.3 + 0.6	S 311		+46.6
Cluster NGC 2467									

Table 9 (continued)

No	l	adopted V _{LSR} (km s ⁻¹)	d _{star} (kpc)	d _{kin} (kpc)	U (pc cm ⁻²)	H109 a source	Ba source	V _{LSR} H109 a (km s ⁻¹)	V _{LSR} Ba (km s ⁻¹)
52	253°8	+31.9	3.1		ε	253.6 - 0.2	RCW 19 RCW 20	+38.3	+28.2 +30.5
		Co D -35°4384 HD 69464 Co D -35°4412 Co D -35°4469 Co D -35°4471							
53	267°9	+ 2.4	1.2		ε	267.8 - 0.9 267.9 - 1.0 268.0 - 1.1	RCW 38 RCW 38 RCW 38	+ 7.8 + 0.0 + 1.8	+ 2.6 + 2.1
54	282°0	+22.0	7.0		m	282.0 - 1.2	[282.0 - 1.2]	+22.4	+21.6
55	284°0	+ 4.5	5.4		ε	284.0 - 0.9	[284.0 - 0.9]	+ 4.5	
56	284°3	- 3.0	4.7		b	284.3 - 0.3	RCW 49	- 0.7	- 5.2
57	285°3	- 1.6	5.2		ε	285.3 + 0.0	H 18	- 1.6	
58	287°6	-21.5	2.6		b	287.2 - 0.7 287.3 - 0.9 287.4 - 0.6 287.5 - 0.6 287.6 - 0.9 287.7 - 0.6 287.8 - 0.8 287.9 - 0.9 287.9 - 0.8	n Car - C 33	-22.4 -17.0 -18.1 -23.6 -24.1 -26.0 -21.3 -20.7 -25.8	-20.9
59	289°1	+27.0	9.2		m	289.1 - 0.4		+27.0	
60	289°9	+21.3	7.9		m	289.8 - 1.1	G 35	+21.9	+20.7
		LSR 2063							
61	291°2	-24.8	2.5		m	291.3 - 0.7	G 38a	-23.4	-26.3
		CPD -60°2583 HD 97319 HD 306097 HD 97499 CPD -60°2641 HD 306196							
62	291°6	+ 8.4	7.2		b	291.6 - 0.5	G 38b	+ 9.4	+ 7.3
		Cluster NGC 3603							
63	291°9	+23.9	9.7		ε	291.9 - 0.7	H 58	+25.5	+22.3
64	294°7	-22.9	2.4		ε	295.1 - 1.6	RCW 62 RCW 61 RCW 60	-20.9	-21.1 -25.4 -24.3
		Cluster IC 2944 HD 100099 HD 99897 HD 99898							
65	298°6	+26.6	11.7		b	298.2 - 0.3 298.8 - 0.3 298.9 - 0.4		+30.6 +25.0 +24.2	
66	305°3	-40.2	2.5		m	305.1 + 0.1 305.2 + 0.0 305.2 + 0.2 305.4 + 0.2 305.6 + 0.0		-37.9 -40.0 -39.1 -39.1 -44.7	
		HD 114478 LSR 2986							
67	308°7	-44.5	2.7		ε	308.6 + 0.4 308.7 + 0.4 (307.6 - 0.3)	RCW 79 RCW 79 (RCW 78) (RCW 80) (RCW 82)	-51.8 -46.4 -38.7	-42.9 -36.3 -48.9 -46.9
		HD 117797 (RCW 78) d = 2.2 kpc LSR 3160 (RCW 80) d = 2.4 kpc							
68	311°5	-64.1	8.5		m	311.5 + 0.4 311.6 + 0.3		-64.8 -63.5	
69	311°9	-46.4	10.7		m	311.9 + 0.1 311.9 + 0.2		-47.3 -45.5	
70	314°2	-50.5	10.9		m	314.2 + 0.4		-50.5	
71	316°8	-36.1	12.5		b	316.8 - 0.1	[316.8 - 0.1]	-36.1	
72	317°1	-47.1	11.9		m	317.0 + 0.3 317.3 + 0.2		-47.4 -46.8	
73	319°2	-22.8	13.7		m	319.2 - 0.4		-22.8	
74	319°4	-14.1	14.2		m	319.4 + 0.0		-14.1	
75	320°3	- 7.7	14.9		m	320.3 - 0.2		- 7.7	
76	320°3	-67.7	5.1		ε	320.3 - 0.3		-67.7	
77	321°0	-60.6	4.2		ε	321.0 - 0.5 321.1 - 0.5	RCW 91 RCW 91	-61.6 -55.5	-62.6
78	322°2	-54.1	3.5		ε	322.2 + 0.6	RCW 92	-51.8	-56.4
79	324°2	-86.6	8.1		ε	324.2 + 0.1		-86.6	

No	l	adopted V _{LSR} (km s ⁻¹)	d _{star} (kpc)	d _{kin} (kpc)	U (pc cm ⁻²)	H109 a source	Ba source	V _{LSR} H109 a (km s ⁻¹)	V _{LSR} Ba (km s ⁻¹)
80	326°6	-40.6		2.5	ε	326.5 + 0.9 326.7 + 0.6	RCW 94 [326.6 + 0.5] RCW 95 [327.0 + 0.5]	-39.0 -44.5	-41.3 -43.8 -39.5 -38.6
81	328°0	-46.2	2.6		m	327.3 - 0.5 328.2 - 0.6 328.0 - 0.1	RCW 97 [328.1 - 0.5] RCW 98 RCW 99 RCW 96 [328.5 - 1.0]	-46.8 -42.9 -44.7	-49.2 -42.0 -40.1 -47.8 -51.5 -47.7
		CPD -53°6768 HD 142468 RCW 38 CPD -54°6846 HD 142565 HD 142634 CPD -53°6950 HD 142152 CPD -54°6991 CPD -54°6807							
82	327°6	-69.8		11.3	m	327.6 - 0.4		-69.8	
83	328°3	-96.2		8.5	m	328.3 + 0.4		-96.2	
84	331°2	-66.0		12.1	m	331.3 - 0.3 331.1 - 0.5		-64.4 -67.7	
		group no 2 (Table 7)							
85	331°7	-86.6		7.8	b	331.0 - 0.2 331.3 - 0.2 331.4 + 0.0 331.5 - 0.1 333.1 - 0.1		-89.2 -84.4 -79.0 -88.7 -90.8	
		group no 1 (Table 7)							
86	332°*	-53.1		4.2	b	330.9 - 0.4 332.2 - 0.5 332.5 - 0.1 332.7 - 0.6 332.8 - 0.6 333.0 - 0.4 333.1 - 0.4 333.3 - 0.4 333.6 - 0.1 333.6 - 0.2 333.7 - 0.5	[332.5 - 0.1] RCW 106 [333.1 - 0.6]	-56.1 -55.0 -55.9 -47.0 -57.2 -53.8 -55.8 -50.1 -53.7 -48.3 -49.9	-52.0 -47.0 -58.3 -50.0
		HD 146919 HD 147049 CoD -51°9977 CoD -51°9979 CoD -51°9984 HD 147419 HD 147318 HD 147331 HD 147359 HD 147617 CoD -50°10372							
		group no 3 (Table 7)							
		RCW 102 RCW 104							
		[332.1 - 1.2] [331.3 - 2.0] [332.5 - 1.9] [332.4 - 1.0]							
		-60.8 -54.3 -54.8 -46.2							
87	335°8	-52.1		4.6	ε	335.8 - 0.2		-52.1	
		group no 8 (Table 7)							
88	336°5	-19.9	1.3		ε	336.5 - 1.5	RCW 108	-24.9	-19.9
		group no 9 (Table 7) Cluster NGC 6193							
89	336°9	-74.9		6.7	m	336.8 + 0.0 336.9 - 0.1 337.1 - 0.2 (337.3 - 0.1)		-78.9 -73.1 -72.7 (-53.5)	
		group no 4 (Table 7)							
90	337°9	-40.4		3.7	ε	337.9 - 0.5		-40.4	
		group no 7 (Table 7)							
91	338°0	-46.9		14.1	b	337.6 - 0.0 338.0 - 0.1 338.1 - 0.1 338.1 - 0.2 338.4 + 0.0		-54.8 -52.5 -41.7 -47.7 -36.9	
		group no 5 (Table 7)							
92	338°4	-4.3		18.0	m	338.4 - 0.2		-4.3	
		group no 6 (Table 7)							
93	338°9	-40.0		14.8	m	338.9 - 0.1		-40.0	
94	338°9	-63.0		6.0	ε	338.9 + 0.6		-63.0	
95	340°3	-43.3		14.4	m	340.3 - 0.2		-43.3	
96	343°5	-30.3		15.6	m	343.5 - 0.0		-30.3	
97	345°5	-18.3	2.0		ε	345.0 + 1.5 345.2 + 1.0 345.3 + 1.5 345.4 + 1.4	[345.0 + 1.5] [345.2 + 1.0] [345.3 + 1.5]	-17.4 - 9.4 -15.5 -14.6	-18.5 -12.8 -17.9 -24.2 -24.3 -18.5
		Clustera Tr 24 NGC 6231							
		IC 4628 [342.7+3.2] RCW 113 [342.8+0.0] IC 4628 [344.9+1.7]							
98	348°8	-20.0		3.5	m	345.5 - 1.0 348.2 - 1.0 349.8 - 0.6 351.7 - 1.2	RCW 117 [349.8 - 0.6]	-21.1 -23.3 -18.9 -25.8 -12.2	-19.8 -26.5
99	351°4	-6.2	1.5		ε	351.4 + 0.7	RCW 126 RCW 127 RCW 128	-2.5 -3.2	-7.9 -7.0 -5.9
		HD 319703 HD 156738 HD 319699 HD 319702 LSR 4093							
100	353°1	-5.1	1.1		ε	353.1 + 0.3 353.1 + 0.7 353.2 + 0.9	RCW 131	-3.8 -2.9 -3.3	-4.1 -6.6 -3.8
		HD 319718 HD 157504 HD 319788							

Table 10. Criteria used to resolve the distance ambiguity

No of criteria see § II, 4	No of the H II complexes in Table 9
(1)	1, 2, 8, 9, 11, 56, 57, 58, 61, 64, 66, 67, 81, 86, 88, 97, 99, 100
(2)	10, 25, 30, 77, 78, 80, 98
(3)	4, 12, 14, 15, 18, 26, 27, 71, 91, 92, 95, 96
(4)	29, 69, 70, 72, 73, 74, 75
(5)	24, 94
(6)	3, 5, 6, 7, 13, 23, 28, 87, 89, 90
(7)	31, 68, 76, 82, 84, 85, 93
other (see § VI, 1, b)	16, 20, 21, 22

constitute a true spiral arm but rather a spur or a branch such as are seen in M 51 and M 101. At the present time it is not yet possible to decide if it is a branch of the Perseus arm of the Sagittarius-Carina arm. The resulting spiral pattern has two symmetrical pairs of arms (i.e. four altogether) with a pitch angle between 10° and 15° .

In the same Fig. 11 we have hatched the five longitudes corresponding exactly to the flux maxima in the radio continuum and in the total 21 cm profile integral: Sagittarius ($\ell = 50^\circ$), Scutum ($\ell = 33^\circ$), Norma ($\ell = 327^\circ$), Crux ($\ell = 305^\circ$), and Carina ($\ell = 283^\circ$) as described by Kerr and Kerr (1970) and Simonson (1970).

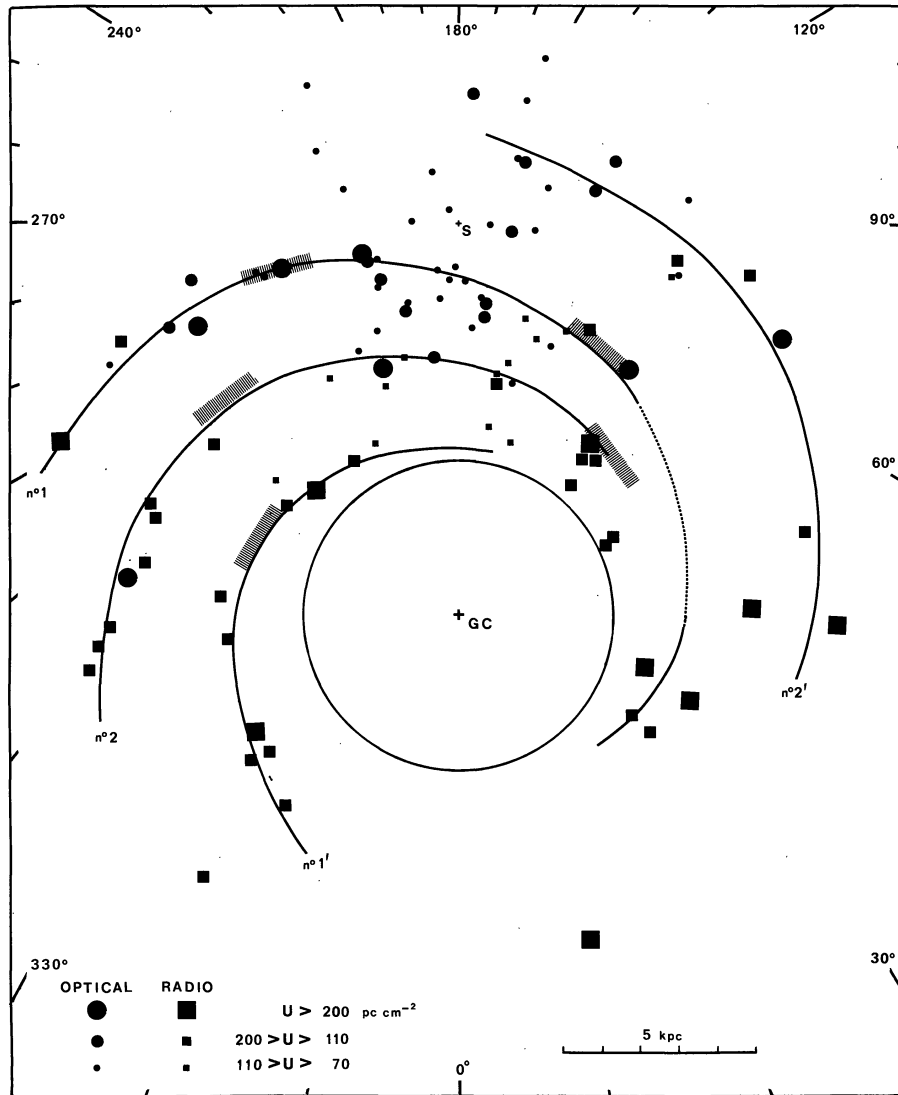


Fig. 11. Spiral model of our Galaxy obtained from high-excitation-parameter H II regions ($U > 70 \text{ pc cm}^{-2}$); the resulting spiral pattern has two symmetrical pairs of arms (i.e. four altogether). No. 1. Major arm: *Sagittarius-Carina arm*; No. 2. Intermediate arm: *Scutum-Crux arm*; No. 1'. Internal arm: *Norma arm*; No. 2'. External arm: *Perseus arm*. Hatched areas correspond to intensity maxima in the radio continuum and in neutral hydrogen

a) Major Arm: Sagittarius-Carina Arm (Arm No. 1)

Optical data (OB clusters, exciting stars, H α velocities) have always suggested that the regions of Sagittarius and those of Carina were parts of the same, rather inclined, spiral arm (Becker, 1963; Lynga, 1964; Georgelin and Georgelin, 1970). The prolongation of this spiral arm out to 9 kpc in Carina has been shown by Bok *et al.* (1970) from optical and radio (H 109 α) data; his sketch shows a spiral arm of more moderate inclination. The high number (Fig. 11) of large brilliant H II regions (optical and radio) which define this Sagittarius-Carina arm shows that we are dealing with a major spiral arm of our Galaxy, in Bok's (1970) sense. As we have already seen, the extreme limit of this principal arm is, optically, the H II region 291.9–0.7 at 9.8 kpc and, in H 109 α , the complex 298.6 (No. 65) at 11.7 kpc. Passing along the arm from its extremity ($\ell = 299^\circ$, $r = 11.7$ kpc) through the optically very well defined tangential point ($\ell = 282^\circ$, $r = 5$ kpc), and up to the regions nearest the Sun ($\ell = 295^\circ$, $r = 2.4$ kpc), the experimentally traced arm is well represented by a logarithmic spiral with a 10° inclination. From longitude 295° to 350° the inclination increases to 15° . For longitudes 0° to 18° , this arm is continued by the very large optical regions M 8, M 20, S 35, S 41, S 44, M 16, M 17 and S 54, at a mean distance of 2.2 kpc. The kinematic distances of small H II regions (S 57, S 58, S 59, S 60, S 61, S 66, S 69 and S 72) with $U < 70$ pc cm $^{-2}$ (except for S 72) allow one to follow this arm between longitudes 22° and 36° (Georgelin *et al.*, 1973). Beyond this point, because of absorption, the optical data cannot be used to follow the arm. Radio data, in particular from the following H II regions, are used:

- W 48 (35.2–1.7) at a distance of 3.0 kpc according to the H 109 α , H $_2$ O, OH, H $_2$ CO and H I results;
- 34.3+0.1—a source linked to W 44, a supernova remnant—located at 3.6 kpc;
- W 51 (No. 30 in Table 9), at $\ell = 49^\circ$ and $r = 5.8$ kpc (see § IV, 2c) which defines the second longitude limit of this spiral arm.

In this part of the arm, the inclination of the spiral arm remains large (14° —see Fig. 11).

In Fig. 11, between $\ell = 330^\circ$ and $\ell = 20^\circ$, this arm is not well-defined and is not clearly separated from the inner Scutum-Crux arm. In fact the outline of the Sagittarius arm is better defined when the smaller regions ($U < 70$ pc cm $^{-2}$) are taken in account (Cramp-ton and Georgelin, 1975, Fig. 1, p. 319). Furthermore, if we plot, in the velocity-longitude diagram, the radial velocities of the 24 H α regions observed between $\ell = 0^\circ$ and $\ell = 30^\circ$, we notice that 22 of them are along a slope of 1.36 km s $^{-1}$ per degree of longitude, with a standard deviation of 3.75 km s $^{-1}$. The velocities of S 48 and S 53 with deviations of 13.8 and 23 km s $^{-1}$ respectively, are clearly not part of this continuity of radial velocity. These two regions lie in the Scutum-Crux arm with other H 109 α sources. Finally, in this sector only two

regions—RCW 98 (No. 81) and RCW 94 (No. 80)—are situated between the spiral arms.

b) Intermediate Arm: Scutum-Crux Arm (Arm No. 2)

From $\ell = 310^\circ$ to $\ell = 325^\circ$ one notes the presence of nine H 109 α groups detected only in radio. One can see in Table 10 that for 7 of these 9 H II regions we have strong certainty of the “far” distances, since if the sources were at the “near” distances (about 2 kpc) they would be detected optically. For 316.8–0.1 absorption lines at greater velocities have been detected in H I and in CH $_2$ O, which confirms the distant hypothesis (Table 4).

Table 9 shows that the sources 320.3–0.3 have a velocity which is not continuous with the others; therefore we choose the “near” solution for it.

These regions form the exterior part of a spiral arm whose tangential point is at about 310° longitude. Towards the interior, one can follow this spiral arm by numerous optical and radio H II regions, in particular:

- the three optical H II regions RCW 91, RCW 92, and [324.1–0.9] which are associated with three (two with RCW 91, one with RCW 92) H 109 α sources (Georgelin, 1970);
- the important field (around RCW 102) of six brilliant optical nebulae associated with eight radio sources (§ V, 1) and
- the four H II regions (only three H α regions) near RCW 117 and RCW 121 which have already been studied in detail (Georgelin, 1975).

The concentration of OB stars at $\ell = 328^\circ$ and $r = 5000$ pc, found by Muzzio and McCarthy (1973), are part of this arm. On the other side of the galactic center one can continue to follow the outline of this spiral arm. Two optical H II regions, S 48 and S 53, are situated beyond the major arm, at 3.5 and 4.3 kpc. These optical H II regions are not the only ones since several large radio complexes are located at neighboring longitudes and distances:

- W 30 (8.1+0.2), with a H 109 α velocity of $+19.3$ km s $^{-1}$ and an OH velocity of $+17.8$ km s $^{-1}$, at 3.4 kpc; ($U < 70$ pc cm $^{-2}$)
- W 33 (12.8–0.2), placed at 4.2 kpc from its H 109 α , CH $_2$ O and H I velocities; and similarly
- 14.6+0.2 and 19.7–0.2 at 4.0 and 3.8 kpc.

After this spiral feature, at 4.1 kpc, we can see in Fig. 11, between $\ell = 8^\circ$ and $\ell = 20^\circ$, three H II complexes (Nos. 20, 21, 22 in Table 9) with radial velocities between 92 and 101 km s $^{-1}$. These radial velocities are very similar to the subcentral velocity and since the radial velocities of the absorption components are not sufficiently different, it is difficult to discriminate between the “near” and “far” distances. However, for 30.8–0.0 (W 43) Radhakrishnan *et al.* (1972, p. 117) has shown that the H I absorption is definitely cut off well before

the tangential-point velocity, and we therefore adopt the "near" distances (6.9, 7.0 and 6.6 kpc) for these three H II regions.

This spiral arm—*Scutum-Crux arm*—is very well represented by a spiral of 12° inclination (see Fig. 11) which can be traced over 150° around the galactic center.

c) Internal Arm: *Norma Arm* (Arm No. 1')

The more internal regions of the Galaxy are too far away from the Sun for one to be able to use optical observations. We have therefore used radio results, and in particular those for H 109 α sources. These sources are intense and "important", i.e., the selection effect is analogous to that made in observations of the optical outline of external galaxies, which in fact define what are called the arms of a galaxy.

We have seen (§ V, Fig. 10) that the radio sources at longitudes 332° and 337° (Mezger, 1970) would define a spiral of 12° inclination. The other H II regions observed between 325° and 15° confirm the outline of this spiral arm.

These are

— $328.3+0.4$ and $327.6-0.4$, both in the vicinity of the tangential point of this arm,

— $338.9-0.1$, at 14.8 kpc,

— $340.3-0.2$, with $V_{\text{H } 109\alpha} = -43.3 \text{ km s}^{-1}$ and OH absorption lines at -40 and -87 km s^{-1} (Caswell and Robinson, 1974, p. 616, Fig. 27 and p. 624); therefore we adopt the "far" distance,

— $343.5-0.0$, which is the most distant H II region observed in this spiral arm

— $338.9+0.6$, at 6 kpc, and

— $8.5-0.3$ and $13.2+0.0$, at 5.3 and 5.8 kpc.

Given the number and "importance" of the H II regions which constitute it, we consider this *Norma arm* to be a major arm of the same kind as the *Sagittarius-Carina arm*. In external galaxies one can observe that the spiral arms are generally symmetrical in the inner region ($R \sim 5$ kpc). Here also, one can see (Fig. 11) that the outline of an arm exactly symmetrical to the *Norma arm* (arm No. 1') corresponds exactly to the prolongation of the *Sagittarius-Carina arm* (arm No. 1).

d) Perseus Arm (Arm No. 2')

As we have restricted ourselves to "important" H II regions ($U > 70 \text{ pc cm}^{-2}$), the well-known Perseus arm is now very tenuous and inconspicuous (Fig. 11). Nevertheless this spiral feature is well established from a great number of faint H II regions, OB clusters and exciting stars (§ IV, 1). From H I results the *Perseus arm* is one of the most striking feature in the 21-cm profiles, this fact is not in contradiction with the H II results. This is a normal difference well known in other galaxies where H I arm are strong at the outside of the

galaxy while H II regions are inconspicuous (Bok, 1971; Monnet, 1972; Burton, 1976).

Between $\ell = 80^\circ$ and $\ell = 40^\circ$ the most important H II regions observed are:

— S 106, $75.8+0.4$, and a complex H II region composed of $79.8+1.2$ and $80.0+1.5$ (Table 9, No. 36) at 5.8, 5.7 and 5.7 kpc;

— $79.3+1.3$ (DR 7), as discussed in § IV, 2, d. The distance is 7.6 kpc;

— $70.3+1.6$ (W 58) an important optical and radio complex discussed previously in § IV, 2, d;

— and the W 49 A complex at 14.1 kpc, the last H II region observed in this spiral arm.

The pitch angle of this arm is about 12° . If we extend the *Perseus arm* (arm No. 2') to the interior with the same inclination, this part is exactly symmetrical with the *Scutum-Crux arm* (arm No. 2).

The spiral scheme which we present here does not attempt to resolve all problems, and of course there are still unresolved points. For example: the two regions RCW 94–95 and RCW 97–98 remain in an interarm (Rydgren, 1974), W 47 is exactly in an interarm, $338.4-0.2$ is between *Scutum-Crux arm* and *Norma arm*, etc.

2. Discussion

a) Compatibility of the Present Model with the Radio Continuum Flux Distribution as a Function of Longitude

We have calculated the flux corresponding to the above-defined spiral model and compared it with the true observed flux in order to test the model. Figure 12 shows the results of this comparison. At the top is the histogram drawn by Kerr and Kerr (1970) based on the Parkes 11 cm data; the bottom histogram has been calculated with our spiral model, with arms 900 pc wide and an intensity 1.5 times greater for the interior arm. The latter histogram is obviously more regular since it assumes uniform and homogeneous arms, but the general form of the observed histogram is reproduced—in particular the two abrupt increases at 304° and 326° , which correspond to the longitudes where the line of sight begins to cross the *Scutum-Crux arm* and the *Norma arm* respectively. The three maxima correspond to the three arms: *Sagittarius-Carina*, *Scutum-Crux* and *Norma*.

b) Compatibility of the Present Model with the Integrated 21-cm Profile as a Function of Longitude

An important result from the 21 cm observations of the spiral structure concerns the directions of the tangential points of the spiral arms (Kerr, 1970; Burton and Shane, 1970; Simonson, 1970). It is therefore indispensable to compare these with the tangential points of our model.

Table below shows that the agreement is very good

21 cm	283°	305°	327°	33°	50°
Proposed model	285°	308°	328°	—	47°

c) Comparison of this Spiral Model with H I Spiral Models

Currently there are two different 21-cm models, given by Kerr (1969) and by Weaver (1970). A comparative discussion of these two models was held at the IAU *Symposium 38* (1970) on the structure of the Galaxy, as well as at the Maryland Spiral Workshop (Simonson, 1970). As we have already seen, the first result of the 21 cm observations is to indicate the longitudes where one sees the arms along the line of sight. In the Kerr model the principal spiral arms are seen tangentially at six longitudes—33°, 50°, 75°, 283°, 305° and 327°—and these tangential points are connected in pairs to form quasi-circular arms. Weaver distinguishes only two tangential directions at $\ell = 50^\circ$ and $\ell = 283^\circ$, paired to form a single principal arm with an inclination of $12^\circ.5$. For other directions, Weaver shows only spurs or minor branches. We have seen that in our model the spiral arms are seen tangentially at the same longitudes as in radio, and in this sense it is compatible with both the Kerr and Weaver models. Ours differs from the Kerr model in that our model connects the arms seen at longitudes 33° and 56° with those seen at 305° and 283° respectively, and not with those at 327° and 305°. To support his interpretation Kerr (Kerr and Kerr, 1970) show that low values of flux in the 11 cm continuum are seen from $\ell = 292^\circ$ to $\ell = 304^\circ$ which give some evidence for a gap between the Carina and Sagittarius features; but in fact in the Sagittarius-Carina arm there is no lack of optical H II regions (Georgelin and Georgelin, 1971; Monnet, 1974, and this paper Fig. 11). Our model differs from that of Weaver by the Scutum-Crux arm and the Norma arm which are totally absent from his model for $300^\circ < \ell < 360^\circ$, but agrees for arms Nos. 1 and 2'.

Compared to the first optical models of Becker (1963), Lynga (1964), and Courtès *et al.* (1970), the present model covers the almost entire Galaxy instead of being limited to about 3 kpc. The arms have an inclination of 10° to 12° instead of 20° and even 25° . This is due partly to the fact that the local feature was indeed highly inclined and now we not consider the local arm (Ori spur) as a part of the general spiral pattern. In addition, the strong interstellar absorption in Aquila hinders the detection of H II regions for $\ell > 20^\circ$, and this had the effect of exaggerating the slope of the Sagittarius arm.

Our model remains an "optical" model insofar as the distance scale is that of the stars and the rotation model is defined by optical data; this is radio model only insofar as it uses H 109 α velocities, made compat-

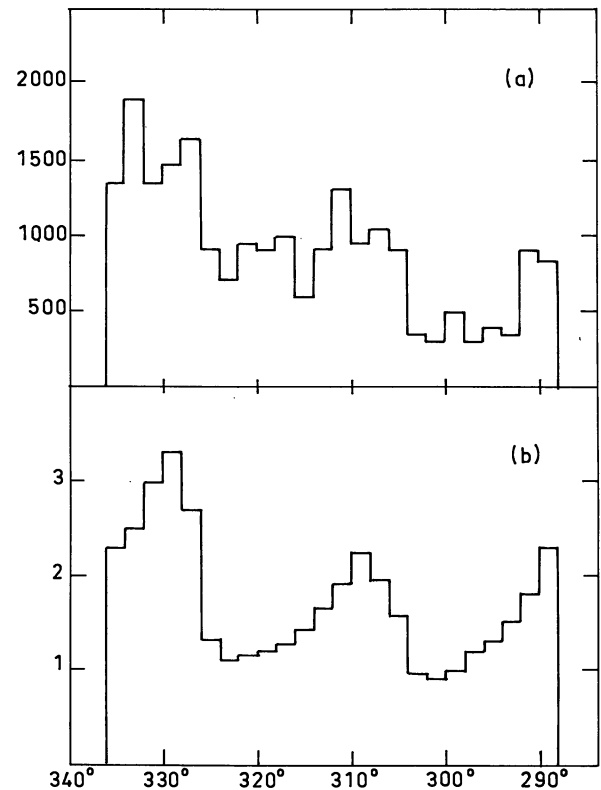


Fig. 12. (a) Flux observed at 11 cm as a function of galactic longitude according to Kerr and Kerr (1970). (b) Flux (on an arbitrary scale) calculated from the four-arm spiral model (Fig. 11) for uniform arms of 900 pc width

ible with the optical data, for H II regions in the interior parts of the Galaxy.

d) Morphological Type of the Galaxy

Determined from the Arms. In Fig. 11 we have indicated all the H II regions whose excitation parameter U was greater than 70 pc cm^{-2} so as to retain only the "important" H II regions, i.e., similar to those observed in external galaxies and which are known to define spiral arms. Figure 11 shows that our Galaxy has four principal arms, well distinct and rich in brilliant H II regions, which undoubtedly gives it a type much closer to Sc than to Sb.

Determined from the Nuclear Bulge. Arp (1965) has shown that for the same surface brightness the bulge of our Galaxy is two times smaller than that of M 31, which places our Galaxy closer to an Sc. Also, Van den Bergh (1968) has shown that the zone of surface brightness $\sigma = \sigma_0$ is located at $R = 12 \text{ kpc}$ in M 31, at $R = 4 \text{ kpc}$ in M 33, and at $R = 8.7 \text{ kpc}$ in our Galaxy. Therefore, this criterion classifies our Galaxy as intermediate between Sb and Sc, whereas the arm criterion is clearly in favor of Sc. Note especially that, in contrast to M 31, large H II regions in our Galaxy are observed at 4 kpc from the center.

As examples of galaxies to which ours may be compared one may cite NGC 6814, NGC 628, NGC 309, NGC 1232 and NGC 5364.

In conclusion, from H II regions one obtains a four-arm spiral pattern with a pitch angle of 12° and symmetrical arms.

Will this pattern perhaps be the long-desired basic diagram of the galactic distribution of gas and young stars? This depends on future observational data and on the determination of crucial facts which, in the next few years, will confirm or disprove this working diagram.

Acknowledgements. We are grateful to Dr. G. Monnet for helpful and stimulating discussion throughout this investigation, to Mme A. Robin for technical assistance with numerous aspects of this work and to J. Caplan for English translation.

References

- Arp, H.C., (and Baade, W.) 1964, *Astrophys. J.* **139**, 1027
 Arp, M.C. 1965, *Astrophys. J.* **141**, 43
 Balona, L., Crampton, D. 1974, *Monthly Notices Roy. Astron. Soc.* **166**, 293
 Balona, L.A., Feast, M. 1974, *Monthly Notices Roy. Astron. Soc.* **167**, 621
 Becker, W. 1963, *Z. Astrophys.* **57**, 117
 Becker, W., Fenkart, R. 1971, *Astron. & Astrophys. Suppl.* **4**, 241
 Bigay, J.H., Garnier, R., Georgelin, Y.P., Georgelin, Y.M. 1972, *Astron. & Astrophys.* **18**, 301
 Bok, B.J. 1970, *IAU Symp.* **38**, 457
 Bok, B.J., Hine, A.A., Miller, E.W. 1970, *IAU Symp.* **38**, 246
 Bok, B.J. 1971, Observational Evidence for Galactic Spiral Structure, *IAU Highlights of Astronomy Vol. 2*, Ed. Cornelis de Jager, Reidel Publ. Co., Dordrecht, p. 63
 Boulesteix, J., Courtès, G., Laval, A., Monnet, G., Petit, H. 1974, *Astron. & Astrophys.* **37**, 33
 Burton, W.B., Shane, W.W. 1970, *IAU Symp.* **38**, 397
 Burton, W.B. 1973, *Publ. Astron. Soc. Pacific* **85**, 679
 Burton, W.B. 1976, *Ann. Rev. Astron. & Astrophys.* **14**
 Burton, W.B., Bania, T.M. 1974, *Astron. & Astrophys.* **33**, 425
 Caswell, J.L. 1972, *Australian J. Phys.* **25**, 443
 Caswell, J.L., Robinson, B.J. 1974, *Australian J. Phys.* **27**, 597
 ChuKit, M. 1973, *Astron. & Astrophys.* **22**, 69
 Conti, P.S., Alschuler, W.R. 1971, *Astrophys. J.* **170**, 325
 Courtès, G. 1960, *Ann. Astrophys.* **28**, 683
 Courtès, G., Carranza, G., Georgelin, Y.P., Monnet, G., Pourcelot, A. 1968, *Ann. Astrophys.* **31**, 63
 Courtès, G., Georgelin, Y.P., Georgelin, Y.M., Monnet, G. 1970, *IAU Symp.* **38**, 205
 Crampton, D. 1971, *Astron. J.* **76**, 260
 Crampton, D., Fisher, W.A. 1974, *Publ. Dominion Astrophys. Obs. Victoria* **14**, 12
 Crampton, D., Georgelin, Y.M. 1975, *Astron. & Astrophys.* **40**, 317
 Danver, C. 1942, *Ann. Obs. Lund* **10**, 1
 Dickel, J.R., Milne, D.K. 1972, *Australian J. Phys.* **25**, 539
 Dickinson, D.F., Frogel, J.A., Persson, S.E. 1974, *Astrophys. J.* **192**, 347
 Dubout, R. 1975, *Astron. & Astrophys. Suppl.* (sous presse)
 Georgelin, Y.P. 1970, *Astron. & Astrophys.* **7**, 322
 Georgelin, Y.M. 1975, Thesis, University of Marseille
 Georgelin, Y.M. 1975a, *Compt. Rend. Acad. Sci. Paris* **280**, série B, 349
 Georgelin, Y.P. 1976, in preparation
 Georgelin, Y.P., Georgelin, Y.M. 1970, *Astron. & Astrophys.* **7**, 133
 Georgelin, Y.P., Georgelin, Y.M. 1970a, *Astron. & Astrophys. Suppl.* **3**, 1
 Georgelin, Y.P., Georgelin, Y.M. 1970b, *Astron. & Astrophys.* **8**, 117
 Georgelin, Y.P., Georgelin, Y.M. 1971, *Astron. & Astrophys.* **12**, 482
 Georgelin, Y.M., Georgelin, Y.P., Roux, S. 1973, *Astron. & Astrophys.* **25**, 337
 Goss, W.M., Manchester, R.N., Robinson, D.J. 1970, *Australian J. Phys.* **23**, 559
 Goss, W.M., Radhakrishnan, V., Brooks, J.W., Murray, J.D. 1972, *Astrophys. J. Suppl.* **24**, 123
 Hine, A.A. 1971, Catalogue of Nebulae in Carina, Steward Observatory, Tucson, Arizona (June)
 Humphreys, R.M. 1970, *Astron. J.* **75**, 602
 Humphreys, R.M. 1972, *Astron. & Astrophys.* **20**, 22
 Israel, F.P. 1974, private communication
 Kerr, F.J. 1969, *Ann. Rev. Astron. & Astrophys.* **7**, 39
 Kerr, F.J. 1970, *IAU Symposium* **38**, 95
 Kerr, F.J., Kerr, M. 1970, *Astrophys. Letters* **6**, 175
 Lynga, G. 1964, 1965, *Medd. Lunds Astron. Obs. Serie II*, 140–143
 Manchester, R.N., Robinson, B.J., Goss, W.M. 1970, *Australian J. Phys.* **23**, 75, 751
 Maucherat, A. 1975, *Astron. & Astrophys.* **45**, 193
 Mezger, P.G. 1970, *IAU Symposium* **38**, 107
 Minkowski, R. 1946, *Publ. Astron. Soc. Pacific* **58**, 305
 Moffat, F.J., Vogt, N. 1973, *Astron. & Astrophys.* **23**, 317
 Monnet, G. 1971, *Astron. & Astrophys.* **12**, 379
 Monnet, G. 1972, Proceedings of First European Astronomical Meeting Athens, September 4–9, Vol. 3, Ed. Springer-Verlag Berlin-Heidelberg-New York 1974
 Monnet, G. 1974, *IAU Symposium* **60**, 249
 Morgan, W.W., Sharpless, S.L., Osterbrock, D.E. 1952, *Astron. J.* **57**, 3
 Muzzio, J.C., McCarthy, C.C. 1973, *Astron. J.* **78**, 923
 Oort, J.H., Kerr, F.J., Westerhout, G. 1958, *Monthly Notices Roy. Astron. Soc.* **118**, 379
 Pismis, P. 1974, *Rev. Mexicana Astron. & Astrophys.* Vol. 1, avril 1974
 Radhakrishnan, V., Goss, W.M., Murray, J.D., Brooks, J.W. 1972, *Astrophys. J. Suppl.* **24**, 49
 Reifenstein, E.C., Wilson, T.L., Burke, B.F., Mezger, P.G., Altenhoff, W.F. 1970, *Astron. & Astrophys.* **4**, 357
 Roberts, W.W. 1969, *Astrophys. J.* **158**, 123
 Robinson, B.J., Caswell, J.L., Goss, W.M. 1971, *Astrophys. Letters* **9**, 5
 Rydgren, A.E. 1974, *Publ. Astron. Soc. Pacific* **86**, 363
 Schmidt, M. 1965, Stars and Stellar Systems, Galactic Structure, Vol. 5, p. 513, Ed. A. Blaauw et M. Schmidt (Chicago Press, Chicago)
 Shane, W.W., Bieger-Smith, G.P. 1966, *Bull. Astron. Inst. Neth.* **18**, 263
 Shaver, P.A., Goss, W.N. 1970, *Australian J. Phys. Astrophys. Suppl.* **14**
 Simonson, S.C. 1970, *Astron. & Astrophys.* **9**, 163
 Smith, B.M. 1972, Catalogue of Nebulae in Crux, Centaurus, Circinus and Norma, Steward Observatory, Tucson, Arizona (September)
 Van den Bergh, S. 1968, *J. Roy. Astron. Soc. Can.* **62**, 145
 Walborn, N.R. 1972, *Astron. J.* **179**, 519
 Weaver, H.F. 1970, *IAU Symposium* **38**, 126
 Whiteoak, J.B., Gardner, F.F. 1970, *Astrophys. Letters* **5**, 5
 Wilson, T.L. 1972, *Astron. & Astrophys.* **19**, 354
 Wilson, T.L., Mezger, P.G., Gardner, F.F., Milne, D.K. 1970, *Astron. & Astrophys.* **6**, 364
 Y. M. Georgelin
 Y. P. Georgelin
 Observatoire de Marseille
 2, place Le Verrier
 F-13004 Marseille, France

Note added in proof. Recently, on december 1975, Caswell *et al.* (1975) obtained new H I absorption radial velocities for H II regions with high emission measure. For these H II regions, the choice between "near" and "far" kinematical distances deduced from H I absorption components is in agreement with our results for 12 H II regions

(Nos 17, 23, 29, 69, 78, 85, 86, 88, 90, 94, 97, 98) not concluding for two others (Nos 4, 84) and in disagreement for two H II regions (Nos 66, 89); particularly, group 4 (No. 89) is far according H I and CH₂O (Whiteoak and Gardner, 1974) absorption lines whereas we chose the "near" distance from OH absorption lines.